PHA-4/FoxA controls the function of pharyngeal and extrapharyngeal enteric neurons of *C. elegans*

Zion Walker[1,2], Wen Xi Cao[1,2], Eduardo Leyva-Diaz[1,2,3], Mayeesa Rahman[1], Surojit Sural[1,2], Michelle A. Attner[1] and Oliver Hobert[1,2] *

[1] Department of Biological Sciences

[2] Howard Hughes Medical Institute, Columbia University, New York, USA

[3] Present address: Department of Developmental Neurobiology, Instituto de Neurociencias (CSIC-UMH), Sant Joan d'Alacant, Spain

*Corresponding author: or38@columbia.edu

Running title: Transcriptional control of enteric nervous system

Keywords: *C. elegans,* Forkhead transcription factor, enteric nervous system

ABSTRACT

FoxA transcription factors pattern gut tissue across animal phylogeny. Beyond their early patterning function, little is known about whether they control the terminal differentiation and/or function of the fully mature enteric nervous system, the intrinsic nervous system of the gut. We show here that the expression and function of the sole *C. elegans* FoxA homolog, PHA-4, reaches beyond its previously described pioneer factor roles in patterning the foregut. Through the engineering of neuron-specific *cis*-regulatory alleles, Cre-mediated cell-specific knockouts and degron-mediated, temporally controlled PHA-4/FoxA removal in postmitotic neurons, we found that PHA-4/FoxA is required not only to initiate the terminal differentiation program of foregut-associated enteric neurons, but also to maintain their functional properties throughout the life of the animal. Moreover, we discovered novel sites of expression of PHA-4/FoxA in extrapharyngeal enteric neurons that innervate the hindgut (AVL and DVB), a GABAergic interneuron that controls foregut function during sleep (RIS), and a peptidergic neuron, PVT, which we implicate here in controlling defecation behavior. We show that while PHA-4/FoxA is not required for the developmental specification of AVL, DVB, RIS, and PVT, it is required to enable these neurons to control enteric functions. Taken together, *pha-4* is the only transcription factor known to date that is expressed in and required for the proper function of all distinct types of enteric neurons in a nervous system.

INTRODUCTION

The gut of adult animals, subdivided into foregut, midgut, and hindgut, is composed of a multitude of distinct cell types. These include enteric neurons that innervate gut tissue to control various aspects of gut function, most notably, the contraction of gut musculature. The enteric nervous system was initially dubbed the “second brain” of an animal to illustrate its physical separation from the CNS and its autonomous function (Gershon 1998). Similarities in the organization and function of the vertebrate enteric nervous system to the nervous system of comparatively more primitive animals such as cnidarians, have resulted in the enteric nervous system being dubbed the “first brain”, i.e., an evolutionary antecedent of a more complex nervous system (Furness and Stebbing 2018). These evolutionary considerations, as well as the involvement of enteric nervous systems in many aspects of human health and disease (Rao and Gershon 2018), have spurred substantial interest in a better understanding of the developmental programs that specify enteric nervous systems. Notably, while early patterning mechanisms that result in the eventual specification of enteric neurons are relatively well understood in a number of distinct invertebrate and vertebrate animal systems (Hartenstein 1997; Laranjeira and Pachnis 2009; Mango 2009; Sasselli et al. 2012; Nagy and Goldstein 2017), the molecular mechanisms that operate in postmitotic neurons to specify their terminal differentiation program and to maintain their functional features during the life of the animal remain incompletely understood.

FoxA-type forkhead domain transcription factors control the specification of gut tissue across animal phylogeny, ranging from protostomes to deuterostomes (Friedman and Kaestner 2006; Mango 2009; Adler et al. 2014; Annunziata et al. 2019). For example, in the nematode *C. elegans,* expression of the sole FoxA transcription factor orthologue, PHA-4, demarcates all cells in the developing embryo that generate foregut, midgut, and hindgut tissue (Azzaria et al. 1996; Horner et al. 1998; Kalb et al. 1998; Mango 2009; Niu et al. 2011; Ma et al. 2021). Previous genetic loss-of-function studies have firmly established functions of PHA-4/FoxA in all sections of the gut at different stages of embryonic development (Mango et al. 1994; Horner et al. 1998; Kalb et al. 1998; Gaudet and Mango 2002; Mango 2009; Fakhouri et al. 2010). In the fore- and hindgut, *pha-4* functions as an organ selector to control the lineage specification and morphogenesis of these tissues during embryonic patterning. Consequently, loss of *pha-4* results in failure to develop these organs. The organ selector role of PHA-4 critically depends on a phylogenetically conserved pioneer factor function of

PHA-4, which involves nucleosome displacement and RNA Pol II recruitment (Hsu et al. 2015).

In the midgut (intestine), *pha-4* may not have a developmental function (a notion that we probe further in this manuscript), but has a well-documented role in intestinal homeostasis (Panowski et al. 2007; Wu et al. 2018; Torzone et al. 2023). Outside the gut, PHA-4 has only been reported to be expressed in a small number of postembryonically generated cells, which share with the alimentary tract the feature of also forming tubular structures, such as the somatic gonad (Kalb et al. 1998; Updike and Mango 2007; Chen and Riddle 2008). PHA-4 appears to function in the proper differentiation of these cells as well (Ao et al. 2004; Updike and Mango 2007; Chen and Riddle 2008).

We set out to investigate *C. elegans* PHA-4 function because of our overall interest in studying terminal differentiation programs of enteric neurons of the foregut and the hindgut (Hobert et al. 1999; Gendrel et al. 2016; Vidal et al. 2022). Two enteric neurons, AVL (located in the ventral head ganglion) and DVB (located in the dorsorectal ganglion of the tail), which we refer to here as "hindgut enteric neurons" (HENs), innervate the hindgut of the worm to control enteric muscle contraction during defecation (McIntire et al. 1993; Avery and Thomas 1997) (**Fig.1A**). AVL and DVB are GABAergic neurons that are activated by the intestinally released neuropeptide *nlp-40*, which generates all-or-none action potentials in these neurons (Mahoney et al. 2008; Wang et al. 2013; Jiang et al. 2022). The rhythmic activation of AVL and DVB results in the GABA-dependent contraction of electrically coupled hindgut enteric muscles (stomatointestinal, anal depressor, and anal sphincter muscles), leading to the expulsion of gut contents (Thomas 1990; Jiang et al. 2022).

In addition, 20 enteric neurons are located within the foregut of the worm, which we term here "pharyngeal enteric neurons" (PENs)(**Fig.1A**). These 20 neurons can be classified into 14 distinct types based on position, neurite morphology, synaptic connectivity and molecular profile (Albertson and Thomson 1976; Cook et al. 2020; Taylor et al. 2021). Like enteric neurons in all other animal nervous systems, PENs form a densely interconnected, autonomously acting network that controls foregut contraction during feeding behavior known as pharyngeal pumping (Albertson and Thomson 1976; Cook et al. 2020).

All 20 PENs require the Six-type homeodomain transcription factor CEH-34 to acquire their unique terminal properties, with CEH-34 interacting with distinct homeodomain cofactors

to specify the distinct identity of individual enteric neurons (Vidal et al. 2022). We had previously reported that of the many distinct functions of PHA-4 during organogenesis and specification of distinct foregut tissue, one is the proper induction of CEH-34 expression in foregut enteric neurons (Vidal et al. 2022). As we describe here in more detail, PHA-4 is not only expressed during embryonic induction of CEH-34 expression, but its expression is maintained in all enteric neurons throughout postdevelopmental stages into adulthood. Surprisingly, we also discovered previously unnoted and continuous PHA-4 expression in the extrapharyngeal HENs (AVL and DVB), as well as in two other extrapharyngeal neurons, RIS and PVT. RIS was previously shown to control foregut-associated behavior (pharyngeal pumping)(Steuer Costa et al. 2019), and we show here that PVT controls hindgut-associated behavior (defecation).

Postmitotic, postdevelopment expression of PHA-4 in these various enteric function-controlling neuron classes indicates that PHA-4 may have late functions after its earlier functions in foregut organogenesis. Through the engineering of neuron-specific cis-regulatory alleles, Cre-mediated cell-specific knockout, and degron-mediated temporally controlled PHA-4 removal, we show here that PHA-4 function extends beyond an early pioneer function to later postdevelopmental roles within pharyngeal enteric neurons, as well as in the extrapharyngeal neurons that control enteric function. Our analysis reveals that PHA-4 represents the only currently known transcription factor whose expression and function covers the entire set of enteric neurons in an animal nervous system.

RESULTS

Expression pattern of *gfp*-tagged *pha-4*

The expression pattern of *pha-4* throughout the entire animal has been previously analyzed using multicopy reporter transgenes and PHA-4 antibody staining (Horner et al. 1998; Kalb et al. 1998; McKay et al. 2003; Grosshans et al. 2005; Panowski et al. 2007; Chen and Riddle 2008; Riddle et al. 2016). 4D live imaging analysis of a PHA-4 fosmid-based reporter further precisely refined the patterns of PHA-4 expression onset during embryogenesis (Ma et al. 2021) (**Fig.1B,C**). One notable aspect of these previous analyses were the observation of PHA-4 expression in a previously unidentified head and tail neuron in adult animals (Kalb et al. 1998; Panowski et al. 2007; Chen and Riddle 2008)(**Fig.1C**). To confirm all these previous patterns using an independent reagent and to identify the nature of the PHA-4 expressing head and tail neurons, we tagged the endogenous *pha-4* locus with *gfp* using CRISPR/Cas9 genome engineering. The locus was tagged at the 3'end to capture all three isoforms of the *pha-4* locus (**Fig.2A**). Resulting *pha-4(ot946[pha-4::gfp])* animals are viable and appear superficially wild-type, indicating that tagging does not affect gene function.

Expression of this *pha-4* reporter allele precisely recapitulated the previous reported sites of expression of PHA-4 throughout the entire alimentary system, from the arcade cells which attach the foregut to the mouth, to all cells of the foregut, midgut (intestine) and cells associated with the hindgut (**Fig.2B**). Expression initiates at the end of gastrulation and is evident throughout the pharyngeal primordium and the midgut (**Fig.2B)**. While expression in the midgut becomes significantly weaker over the course of embryonic and postembryonic development, *pha-4* expression in cells of the fore- and hindgut remain strong into adulthood (**Fig.2B; Fig.S1A**), a possible consequence of transcriptional autoregulation of the *pha-4* locus (Kaltenbach et al. 2005).

While previous studies noted expression only in an unidentified "head neuron" and a "rectal neuron" (Kalb et al. 1998; Panowski et al. 2007; Chen and Riddle 2008), we noted a total of four extra-pharyngeal neurons that express *pha-4(ot946)* in the adult. Based on position, and with the use of molecular landmarks, we identified these as the GABAergic RIS, AVL and DVB neurons and the peptidergic PVT tail neuron (**Fig.2B-D**). Onset of expression in RIS, AVL and rectal cells, including PVT is observed in the comma stage embryos shortly

after these neurons have been generated, while expression in DVB becomes apparent at the late L1 stage, when DVB is born (**Fig.2B**). All four neurons are known to require a terminal selector transcription factor, the LIM homeobox gene *lim-6*, for their proper differentiation (Hobert et al. 1999; Aurelio et al. 2003; Gendrel et al. 2016); we found that in *lim-6* null mutant adult animals, *pha-4* reporter allele expression is still present in these neurons, but notably weaker, indicating that *lim-6* is required to sustain proper *pha-4* expression expression (**Fig.S1B**).

***pha-4*-expressing extrapharyngeal neurons control enteric behavior**

Three of the four PHA-4-expressing, extrapharyngeal neurons have been previously linked to the control of gut function. The head neuron RIS, whose single axon extends around the isthmus of the pharynx (**Fig.3A**), controls foregut function, as inferred from optogenetic activation of RIS affecting serotonin-induced pharyngeal pumping rate (Steuer Costa et al. 2019). We sought to corroborate the involvement of RIS in controlling pharyngeal pumping by silencing RIS using a transgene of *flp-11*-promoter driving expression of a histamine-gated chloride channel (HisCl) (Grubbs et al. 2020). We found that histamine-induced silencing of RIS in freely moving animals decreases pharyngal pumping behavior, while not having any impact on hindgut-controlled defecation behavior (**Fig.3D**).

AVL and DVB are known hindgut-innervating enteric neurons ("HENs") which control enteric muscle contraction during defecation (McIntire et al. 1993)(**Fig.1A**). The defecation motor program occurs in three steps: contraction of posterior body muscles (pBoc), contraction of anterior body muscles (aBoc), and explusion (Exp) (Thomas 1990). A pacemaker in the intestinal epithelial cells initiates the pBoc step, which acts upstream of AVL and DVB (Dal Santo et al. 1999). The Exp step requires activation of AVL and DVB to constrict hindgut enteric muscles to release gut contents through the anus. The defecation cycle is highly regular both within and across individuals over time, with well-fed young adult animals never missing a pBoc, aBoc, or Exp step (Thomas 1990).

PVT is a peptidergic interneuron in the pre-anal ganglion whose single axon extends from the tail to the isthmus of the pharynx (**Fig.3B**). PVT displays an intriguing lineage relationship with some cellular constituents of the gut (**Fig.1B**), but no function in relation to the enteric system has been previously investigated. To manipulate PVT activity, we first

used scRNA data (Taylor et al. 2021) to identify a potential driver with PVT-specific expression. We focused on the promoter regions of two genes, *cnc-11* and *sre-22*, and found that fusion of each promoter to GFP::H2B resulted in strong expression in PVT. *cnc-11p::GFP::H2B* also showed expression in non-neuronal cells around the vulva and in hypodermal cells, while *sre-22p::GFP::H2B* also shows weak expression in a neuron pair that we tentatively identified as PVQ L/R based on their location anterior to PHA L/R and PHB L/R in the lumbar ganglion (**Fig.3C**). We used the promoter of *sre-22* to drive histamine-gated chloride channel (HisCl) in PVT and found that after histamine-treatment the frequency of pBoc events in such transgenic animals was unaffected, but the rate of expulsions was significantly reduced (**Fig.3E)**. Compared to untreated PVTp::HisCl worms, histamine-treated worms expressing PVTp::HisCl exhibited significantly less expulsion events, with an average of every third pBoc event not followed by an expulsion event (**Fig.3E).** PVT silencing does not affect pharyngeal pumping (**Fig.3E**).

PVT has also recently been shown to control locomotory quiescence during sleep like-behavior via releasing melatonin (Niu et al. 2020). We found that animals lacking the melatonin-synthesizing *homt-1* gene display no effect in defecation behavior (**Fig.3F)**, indicating that PVT may act via other signaling pathways to control defecation behavior. Since PVT expresses a host of neuropeptides (Taylor et al. 2021), we tested whether removal of the neuropeptide-processing enzyme *egl-3* in PVT would affect defecation behavior. To this end, we used a floxed *egl-3* locus (Marquina-Solis et al. 2024) and drove Cre expression with the *sre-22* driver. We found that in worms with *egl-3* removed from PVT, the frequency of pBoc events were still unaffected, but not all pBoc events were followed by expulsions **(Fig.3G).** Worms with *egl-3* removed from PVT displayed both missed expulsions and failed expulsions, in which a weak contraction of the intestinal muscle was observed, but the concerted contraction of the hindgut enteric muscles and expulsion of gut contents was absent (**Supp Video 2**). While the timing of the weak muscle contraction occurs roughly 3 seconds after the pBoc in the defecation cycle, which is typical when AVL and DVB are active, the weak muscle response is not sufficient to complete the expulsion of gut contents from the body (**Supp Video 2)**. Worms expressing only the floxed *egl-3* locus exhibit normal defecation behavior, in which every pBoc is followed by an expulsion step (**Supp Video 1**).The aberrant expulsion phenotype observed in worms with *egl-3* removed from PVT points

towards a potential role of PVT in the neuropeptidergic activation of AVL and DVB during the Exp step of defecation.

The neuropeptide *nlp-40* regulates the calcium transients of AVL and DVB, in order to orchestrate the release of GABA onto the hindgut enteric muscles. *nlp-40* is thought to be secreted from the intestine in response to intestinal calcium waves of the pBoc and aBoc (Wang et al. 2013). Intriguingly, as per scRNA data (Taylor et al. 2021), the most strongly expressed neuropeptide expressed in PVT is *nlp-40*. We validated this observation by engineering a *T2A:gfp::h2b* cassette into the *nlp-40* locus, confirming strong expression in PVT (**Fig.3H**). We also found clear expression of the NLP-40 receptor AEX-2 in PVT using an *SL2::gfp::h2b* cassette (Ripoll-Sanchez et al. 2023), suggesting that NLP-40 release from PVT may cooperate to amplify intestinally released NLP-40 to control the defecation behavior that is disrupted in *nlp-40* mutants (Wang et al. 2013).

***Cis*-regulatory elements driving neuronal PHA-4 expression**

An analysis of *pha-4* function in PENs and HENs, particularly in regard to the control of enteric behaviors, is complicated by (a) the early lethality of *pha-4* null mutants and (b) its expression in multiple distinct cells of the alimentary tract. The dissection of the cis-regulatory architecture of a genetic locus provides a potential avenue to generate *cis*-regulatory mutant alleles in which expression of a gene is lost selectively in only specific subsets of cells that normally express this gene. Previous work had shown that a genomic 7kb fragment that contains around 2kb of sequences of the longest isoform of the *pha-4* locus, as well as several exons and introns, drives *lacZ* reporter expression throughout the entire alimentary tract, while a 300bp fragment upstream of the first isoform drives expression exclusively in the midgut (**Fig.4A**)(Azzaria et al. 1996; Kalb et al. 1998). We recapitulated the intestine-specific expression with a *gfp*-based transgene that captures the region upstream of the longest *pha-4* isoform (*pha-4prom1;* **Fig.4A,B**). Interestingly, 2,242 bp of sequences upstream of the second isoform (i.e. the first intron of the large isoform; *pha-4prom2*) drove exclusive expression of a *gfp* reporter in all PENs and HENs (AVL, DVB), as well as the RIS and PVT neurons (**Fig.4C**). We confirmed this notion by crossing these transgenic animals with red fluorophore transgenes that marks either the entire nervous system or, selectively, the GABAergic identity of the HENs (**Fig.S1C,D**). The onset of expression the of *pha-*

4prom2::gfp transgene in HENs and PENs is comparable to the onset of expression of the endogenously tagged *pha-4* locus (**Fig.4C, Fig.2B**).

Postmitotic enteric neuron expression of PHA-4 is essential for feeding and survival

Based on the *cis*-regulatory analysis described above, we used CRISPR/Cas9 to eliminate the entire first intron of *pha-4a* isoform from the endogenous *pha-4* locus that we had tagged with *gfp* (**Fig.5A**). We found that in these animals, *gfp* expression is selectively depleted from PENs, HENs, RIS, and PVT (**Fig.5B**). Intriguingly, expression in these neurons appears intact initially, but is lost by the 1.5-fold stage and remains absent in L1 animals (**Fig.5B**), raising the possibility that the *pha-4prom2* region represents an autoregulatory element. To test this notion, we crossed two independent, chromosomally integrated *pha-4prom2* reporter lines into a *pha-4* null mutant background. We found that expression is mostly lost from PENs, but usually is still normal in two extrapharyngeal neurons, likely AVL and RIS (**Fig.5C; Fig.S1E**). We conclude that *pha-4* indeed autoregulates in many cell types, albeit apparently not in extrapharyngeal neurons.

Strikingly, animals carrying this *cis*-regulatory allele of *pha-4* display no obvious pharyngeal morphology defects, but arrest development at the first larval stage, as scrawny, starved looking animals, (**Fig.5D**). This is exactly the phenotype expected from loss of function of PENs, specifically, the M4 motor neuron, whose microsurgical removal results in exactly the same L1 arrest phenotype (Avery and Horvitz 1989).

Even though the temporal dynamics of expression of the *pha-4* cis-regulatory allele (loss only in postmitotic neurons) and its resulting larval arrest phenotype already strongly argue for postmitotic neuronal function of *pha-4*, we sought to independently validate this notion, using an orthogonal approach. To this end, we first engineered two loxP sites into the *pha-4* locus (**Fig.5A**). We independently engineered two strains in which we inserted a *FLAG::NLS::Cre::SL2* expression cassette at the 5'end of two different genes, *egl-3* (neuropeptide-processing enzyme) and *ceh-48* (homeobox gene)**(Fig.S2**). We had previously shown through *gfp* tagging of these loci that either loci is expressed exclusively in all postmitotic neurons of the central, peripheral and enteric nervous systems (Leyva-Diaz and Hobert 2022). We crossed *egl-3*$^{SL2::Cre}$ and *ceh-48*$^{SL2::Cre}$ independently with the floxed *pha-4* locus, and confirmed the depletion of *pha-4::GFP* expression in normally *pha-4*-expressing

neurons (**Fig.5E**). In both resulting strains, we observed the same phenotype that we observed upon removal of the *pha-4prom2* elements: In each strain, neuronal expression of PHA-4::GFP is lost by the 2-fold stage and these animals arrest as scrawny, starved-looking L1 with no obvious pharyngeal morphology defects (**Fig.5E**). Taken together, the phenotypes of the *cis*-regulatory allele, as well as the neuron-specific removal of floxed *pha-4* let us conclude that *pha-4* function extends beyond embryonic patterning to a function in postmitotic neurons.

Effect of *pha-4* removal on neuron differentiation

We used both the *cis*-regulatory allele of *pha-4* as well as the postmitotic Cre-mediated excision of the floxed *pha-4* locus to ask whether postmitotic removal of *pha-4* expression affected PEN differentiation. Analyzing *unc-17/VAChT* expression in the *cis*-regulatory allele, as well as *eat-4/VGluT* and *cat-1/VMAT* expression in the floxed *pha-4* allele, showed gene expression defects in cholinergic, glutamatergic and serotonergic PENs (**Fig.6A**). Panneuronal identity, marked by an *unc-75* reporter is unaffected after postmitotic *pha-4* removal (**Fig.6A**), leading us to conclude that *pha-4* participates in regulating the proper identity of PENs, but not their survival.

To assess the impact of *pha-4* on the differentiation of the extrapharyngeal neurons that we newly identified to express *pha-4* (RIS, AVL, PVT, and DVB), we did not rely on neuron-specific removal of *pha-4*, but rather first examined a complete *pha-4* null allele, to assess the strongest possible phenotype. In spite of the overall disorganization of the head region in *pha-4* null mutants, molecular markers for RIS, AVL and PVT are selectively enough expressed to allow for proper assessment of expression in *pha-4* null mutants. For the RIS and AVL neurons, we used terminal function genes previously shown to be critical for the function of these neurons, the vesicular transporter *unc-47/VGAT* (AVL and RIS), the GABA biosynthetic enzyme *unc-25/GAD*, and the neuropeptides *flp-11* (RIS) and *flr-2* (AVL). Expression of these markers is not affected in L1-arrested *pha-4(ot1506)* null mutant animals (**Fig.6B**). Notably, *flr-2* is normally also expressed in PENs (Vidal et al. 2022) and we find PEN expression to be lost in *pha-4* null mutants (**Fig.6B**).

To assess the effect of neuron-specific *pha-4* removal on DVB, which is born after the L1 stage (i.e. after *pha-4* null mutant animals die), we removed *pha-4* cell-specifically from

DVB by driving Cre recombinase under control of the GABA neuron-specific promoter of the *unc-47/VGAT* locus. An *unc-47prom::Cre* miniMOS line indeed removed endogenously *gfp*-tagged *pha-4* from the RIS, AVL and DVB neurons, but not the PVT neurons, as expected (**Fig.7A**). Post-embryonic loss of *pha-4* from DVB does not affect the expression of molecular markers *flr-2*, and *unc-47/VGAT*(**Fig.6B**). However, we cannot exclude the possibility that the Cre-mediated gene removal is too late to affect differentiation of the neurons. Nevertheless, considering the result with the null allele, it appears that in contrast to strong differentiation defects observed in the PENs, the RIS, AVL, and DVB neurons are generated and appear to adopt their proper fate in the absence of *pha-4* function.

In the PVT neurons, *pha-4* appears to play an earlier patterning role. PVT is the sister of rectal cells that Mango and colleagues had noted to be absent in *pha-4* mutants (Mango et al. 1994). Consistent with a lineage defect, we find that in *pha-4* null mutants, expression of a terminal marker for PVT identity, *sre-22*, is frequently lost, as is expression of a reporter allele of the *pdf-1* neuropeptide (**Fig.6C**). The *nlp-40* neuropeptide reporter allele shows reduced expression in a tail cell outside of the pre-anal ganglion region, where PVT normally resides (**Fig.6C**). We further corroborated a potential lack of functional PVT by examining the expression of a regulator of PVT identity, the LIM homeobox gene, *lim-6* (Hobert et al. 1999; Aurelio et al. 2003). We find no observable *lim-6* signal in the tail region (**Fig.6C**), consistent with a loss of the PVT neuron.

We also examined the impact of *pha-4* on the rectal epithelial K cell, which is lineally related to PVT (**Fig.1B**), and the precursor of the postembryonically born DVB hindgut innervation neurons. We found that expression of the K cell marker, *egl-38*, is affected in *pha-4* null mutants (**Fig.6C**), again consistent with *pha-4* having early developmental defects in generating components of the hindgut. This is further supported by our analysis of the expression of *aex-5*, which codes for an endopeptidase involved in defecation behavior (Mahoney et al. 2008). An *aex-5* reporter allele that we generated by CRISPR/Cas9 genome engineering (Sural et al. 2025) is expressed in the rectal gland cells (one of which, rectD, also lineally related to PVT; **Fig.1B**) and in intestinal-rectal valve cells (virL/R) and this expression is lost in *pha-4* null mutants (**Fig.6D**).

lim-6 is a terminal selector of AVL and RIS, as well and, again consistent with the lack of differentiation defects of AVL and RIS (Hobert et al. 1999; Gendrel et al. 2016), we find *lim-6* expression in these neurons to be apparently unaffected in *pha-4* null mutants (**Fig.6B**).

Intriguingly, we noted ectopic *lim-6* expression in the head, indicating that pharyngeal cells that fail to differentiate properly in *pha-4* mutants convert their identity in *lim-6(+)* neurons (**Fig.6B**).

Lastly, we found that in *pha-4(ot1506)* null mutants, the expression of several markers of terminal differentiation of intestinal cells (*ges-1* and *aex-5)* is unaffected (**Fig.6D**). Since previous work has shown that *pha-4* is required for proper function and homeostasis of mature intestinal cells (Panowski et al. 2007; Wu et al. 2018; Torzone et al. 2023), we therefore set out to assess whether HENs, even though apparently differentiating appropriately, may also be dysfunctional in the absence of *pha-4.*

pha-4 **acts in GABAergic HENs and in PVT to control defecation behavior**

To avoid the larval lethality associated with either *pha-4* null mutants or with panneuronal removal of *pha-4*, we set out to remove *pha-4* selectively from HENs (AVL, DVB). To this end, we expressed Cre recombinase specifically in GABAergic neurons using the *unc-47/VGAT*promoter. An *unc-47prom::Cre* miniMOS line indeed removed endogenously *gfp*-tagged *pha-4* from the RIS, AVL and DVB neurons, but not the PVT neurons or other rectal, as expected from the specificity of the *unc-47prom* driver (**Fig.7A**). Since AVL and DVB neurons, both motor neurons that innervate enteric muscle, were previously shown to control defecation behavior (McIntire et al. 1993), we analyzed this behavior in animals lacking *pha-4* in GABAergic neurons and indeed observed defecation defects. While the rate of pBoc events in these worms was only mildly affected, not all pBoc events were followed by expulsion events (**Fig.7B; Fig.S3**). In some worms, expulsion events were entirely absent for the six observed defecation cycles **(Fig.7B)**, which is consistent with the phenotype of worms in which AVL and DVB are ablated (Choi et al. 2021). Removing *pha-4* from GABAergic neurons does not affect pharyngeal pumping behavior (**Fig.7B; Fig.S3**).

To assess whether PVT requires *pha-4* to regulate defecation behavior, we employed the PVT driver, *sre-22 promoter* described above to express Cre selectively in the PVT neuron of animals that contain a floxed copy of the *pha-4* locus. These animals also exhibit significant defects in the expulsion step of defecation, with only about half of pBocs being followed by an expulsion step (**Fig.7C**). These defects were similar to those observed upon

selective removal of *egl-3* from PVT (**Fig.3**). We conclude that *pha-4* is required for features of PVT that are critical for its function in controlling defecation behavior.

pha-4 **is continuously required to sustain function of HENs and PENs**

While Cre-mediated removal of *pha-4* establishes a function for *pha-4* in postmitotic PENs and HENs, it does not address whether *pha-4* may also function post-embryonically to maintain function of these neurons through to adulthood. Previous work using a temperature-sensitive allele of the *pha-4* locus indicated that *pha-4* removal at the first larval stage resulted in animal lethality (Gaudet and Mango 2002), but it was not clear in which tissue type *pha-4* was required, nor whether this requirement persisted into later stages of animal life. To address this issue, we used the auxin-inducible degron system (Zhang et al. 2015). We tagged the endogenous *pha-4* locus with an auxin-inducible degron (AID) sequence (**Fig.8A**) and generated a transgenic line in which the TIR1(F79G) ligase (Hills-Muckey et al. 2022) is driven in by the *pha-4prom2* driver described above. After addition of the auxin-derivative 5-Ph-IAA, we observe that GFP::loxP::3xFLAG::AID2-tagged PHA-4 is indeed depleted from PENs, AVL and RIS, but not from DVB or PVT (**Fig.8B**)**.** Using this system, we scored feeding and defecation behavior of adult animals that have either been treated since embryonic, L1 or L4 larval stages with 5-Ph-IAA , and we found that PHA-4 is required continuously after embryonic development for maintainance of enteric functions (**Fig.8C**).

DISCUSSION

The role of FoxA genes in gut development is evident across animal phylogeny. Previous studies on the *C. elegans* FoxA ortholog PHA-4 have firmly established its role as an organ selector gene for foregut development (Mango et al. 1994; Mango 2009). Target genes for PHA-4 have been defined during this embryonic patterning function in different parts of the foregut (Gaudet and Mango 2002; Gaudet et al. 2004; Fakhouri et al. 2010) and, on a mechanistic level, PHA-4 has been shown to act as a pioneer factor to enable gene activation (Hsu et al. 2015). We have extended here the description of PHA-4 function by revealing postmitotic functions of PHA-4 during terminal differentiation of enteric neurons, not only of the foregut, but hindgut, as well as other neurons that control the function of the fore- or hindgut. These postmitotic functions extend beyond into larval and adult stages. Since pioneer factors – of which the vertebrate PHA-4 ortholog FoxA is the paradigmatic example - are generally thought to provide the initial trigger for opening chromatin (Zaret and Carroll 2011), a continuous requirement for PHA-4 indicates functions of PHA-4 that go beyond such pioneer function. We propose that continuously expressed PHA-4 cooperates within the foregut enteric nervous system with a previously identified pan-enteric homeodomain transcription factor, the Six-type homeodomain protein CEH-34, that is also required to initiate and maintain enteric neuron differentiation (Vidal et al. 2022). A direct role of PHA-4 in maintaining, together with CEH-34, the fully differentiated state of pharyngeal enteric neurons is supported by the presence of ChIP-Seq peaks for PHA-4 (identified by the ModEncode project; (Gerstein et al. 2010)) in the vicinity of terminal marker genes, including, for example, the *cat-1/VMAT* locus whose expression we find to be affected by postdevelopmental removal of PHA-4.

Perhaps most remarkably, our discovery of expression of PHA-4 in extrapharyngeal neurons points to a fundamental relatedness of HENs and PENs, but also identified other neurons that control the enteric system. PHA-4-expressing AVL and DVB neurons have long been recognized as hindgut innervating neurons that control defecation behavior. The extrapharyngeal RIS interneuron, that we discover here to also express PHA-4, is a known regulator of pharyngeal pumping (Steuer Costa et al. 2019). Even though its cell body is located outside the foregut in the ventral ganglion on its head, the extension of its unipolar process along the nerve ring that wraps around the isthmus of the pharynx, puts RIS in a suitable position to control pharyngeal pumping apparently via the release of neuropeptides

(FLP-11) perceived by neuropeptide receptors expressed in pharyngeal enteric neurons. The expression of PHA-4 in the PVT neuron guided us to explore a potential function of PVT in enteric behavior as well. We discovered that PVT plays a role in controlling the expulsion step of defecation, apparently mediated via neuropeptide release. Removing *pha-4* from PVT using a cell-specific Cre driver recapitulated the expulsion defects seen in worms where PVT was silenced, suggesting that *pha-4* is required for the enteric function of PVT.

Previous work has suggested that the neuropeptide NLP-40 is secreted from the intestine to stimulate proper levels of GABA release in AVL and DVB (Wang et al. 2013). Since we found *nlp-40* to also be very strongly expressed in PVT and since the NLP-40 receptor AEX-2 is expressed not only in AVL and DVB, but also in PVT (Ripoll-Sanchez et al. 2023), it is conceivable that PVT may operate as an amplifier. It may detect NLP-40 released from the intestine via the AEX-2 receptor to promote further NLP-40 release from PVT to stimulate AEX-2 in AVL and DVB during the expulsion step.

With its extension of a long process into the nerve ring from the tail of the animal, PVT represents a potential route of communication from the brain to the hindgut, akin to the vagus nerve. The lineage relationship of PVT with other parts of the hindgut (**Fig.1B**) could have already predicted a function of PVT in controlling hindgut function. Yet, we note that lineage relationships of functionally related neurons are certainly not a universal feature, within the gut (e.g. the hindgut innervating neuron AVL has no lineage relationship to any part of the gut) or outside the gut (e.g. amphid sensory neurons have very limited lineal relationships). Lastly, we note that the function of the peptidergic RIS and PVT neurons in controlling enteric function can be viewed as conceptually similar to the control of vertebrate enteric nervous system function (e.g. gut motility) by neuropeptides produced by the CNS (Furness 2012).

While PHA-4 may act together with (and upstream of) a terminal selector, CEH-34, to control multiple aspects of PENs in a master regulatory manner, PHA-4 function in extrapharyngeal neurons (AVL, DVB, RIS, PVT) may be restricted to controlling select aspects of the functional properties of these neurons. Notably, all these four neurons utilize a shared LIM homeodomain transcription factor for their proper differentiation, *lim-6* (Hobert et al. 1999; Aurelio et al. 2003; Gendrel et al. 2016). In each of these neurons, PHA-4 may assist LIM-6 in controlling some critical aspect of their function. A similarly selective mode of action of PHA-4 in controlling cell function rather than cell differentiation is observed in the midgut endoderm, which also forms properly in *pha-4* mutants, but which displays a number

of functional defects, such as in lipid homeostasis (Wu et al. 2018; Torzone et al. 2023). Hence, PHA-4 acts in a highly contextualized environment. In some cells it acts to control cell differentiation in a “master regulatory manner”, in combination with other transcription factors, while in yet other cell types its function is committed to controlling a highly selective subset of as yet undiscovered genes to control select aspect of their functional properties.

We conclude that PHA-4 is currently the only gene whose expression is tightly restricted to every single neuron of an enteric nervous system, where it fulfills a number of diverse functions from initial fate specification to maintenance of their functionality throughout the life of the animal.

MATERIAL AND METHODS

Strains

All *C. elegans* strains were cultured at 20°C on nematode growth medium (NGM) plates seeded with *Escherichia coli* (OP50 strain) bacteria as a food source unless stated otherwise. The wild-type strain used is Bristol N2. All experiments were performed on hermaphrodites. A comprehensive list of the strains utilized in this study is available in **Table S1**.

Reagents for PVT neuron visualization and manipulation.

To identify drivers for PVT neuron expression, pZW28 [*cnc-11p::gfp::h2b::tbb-2 3'UTR*] was generated by cloning a 757 bp *cnc-11* promoter fragment (-757 to -1 position with respect to the start codon of *cnc-11*). pZW30 [*sre-22p::gfp::h2b::tbb-2 3'UTR*] and pZW32 [*sre-22p:: HisCl::sl2::gfp::tbb-2 3' UTR*] were generated by cloning a 1,144 bp *sre-22* promoter fragment (-1,144 to -1 position with respect to the start codon of *sre-22*). The *tbb-2* 3' UTR sequence is a 156 bp sequence immediately downstream of the stop codon of the *tbb-2* gene. All plasmids used in this study were generated via NEBuilder HiFi DNA assembly using the manufacturer's protocol. All plasmid sequences were validated using Sanger (Azenta) and/or Oxford Nanopore (Plasmidsaurus) sequencing.

Prior to microinjection, all plasmids were linearized using a restriction site in the plasmid backbone. The linearized plasmids were then injected into both gonadal arms of young adult animals. F1 progeny were selected based on the expression of the co-injection marker, and those that transmitted the array to F2 progeny were used to establish transgenic lines. Three independent lines (derived from independently injected P0 animals) for each injection type were utilized in subsequent experiments.

nlp-40 and *pdf-1* expression in PVT, intially suggested by the CeNGEN atlas (Taylor et al. 2021), was examined by inserting an T2A::3xNLS::GFP cassette at the 3' end of the *nlp-40* and *pdf-1* coding sequences (SunyBiotech). This reporter cassette was subsequently shown to produce lower expression than other reporter cassette (Sun et al. 2023), with which

we explain why the *nlp-40* reporter allele shows expression in PVT, but not the midgut, as previously reported (Wang et al. 2013).

Other transgenic lines

Two *pha-4* promoter fragments were used to drive expression of a GFP reporter. pWXC065 [*pha-4prom1::gfp::unc-54 3'UTR*] was generated by cloning a 1963 bp promoter fragment upstream of the longest isoform of pha-4 (-1954 to +9 position relative to the start codon of *pha-4a*). pWXC067 [*pha-4prom2::gfp::unc-54 3'UTR*] was generated by cloning a 2393 bp fragment including nearly the entire first intron of *pha-4a* isoform and up to the second codon of the *pha-4b* isoform (position +53 to +2445 relative to the start of *pha-4a*). These promoter fragments were cloned into the multiple cloning site of the *C. elegans* GFP expression vector pPD95.75 (Fire Vector Kit). Transgenic worms carrying extrachromosomal arrays of these reporter constructs were generated by injecting these plasmids into a *pha-1(ts) allele* alongsite a *pha-1(+)* rescue plasmid, and array-carrying worms were selected for at 25°C.

The *pha-4prom2* fragment was also used to drive additional reagents, namely TIR1(F79G) for auxin-dependent protein degradation (*otIs908*) and GCaMP6s for visualizing activity of enteric neurons (*otIs898*). Table S1 provides full genotypes for these strains. The TIR1(F79G) sequence in pSS35 [*pha-4prom2::TIR1(F79G)::mTur2::tbb-2 3' UTR*] was generated by introducing the F79G [Phe(TTC) to Gly(GGA)] mutation in the *Arabidopsis thaliana* TIR1 sequence, as described previously (Hills-Muckey et al. 2022; Sural et al. 2025).

To drive GCaMP expression with *pha-4prom2* fragment, pWXC072 [*pha-4prom2::3xNLS::ceGCaMP6s::unc-54 3' UTR*] was cloned by swapping out the promoter region of previously published pEY13 [*arrd-4p::3xNLS::ceGCaMP6s::unc-54 3'UTR*] (Yemini et al. 2021), containing the *C. elegans* codon-optimized GCaMP6s sequence. The *arrd-4* promoter was excised by restriction digest by SphI and XmaI, and PCR-amplified *pha-4prom2* promoter fragment was inserted using the HiFi Assembly kit (NEB). Plasmid DNA sequence was validated by Sanger sequencing (Azenta). Both *otIs908* and *otIs898* integrated lines were generated by FLInt-mediated integration, described below.

The *aex-5* reporter allele, as well as the *ges-1prom* reporter lines (which drives expression of a tagged insulin gene) used to assess intestinal fate is described in (Sural et al. 2025).

We generated Cre driver lines in different ways. PVT::Cre (*sre-22p::2xFlag::NLS::Cre::tbb-2 3'UTR, unc-122::gfp*) was generated by amplifying the *2xFlag::NLS::Cre* region from pMA193. The amplified *2xFlag::NLS::Cre* regulatory region was cloned into the pZW30 backbone amplified from the *tbb-2* 3'UTR to the 1,144 bp *sre-22* regulatory region to generate pZW37 *sre-22p::2xFlag::NLS::Cre::tbb-2 3'UTR*. Before microinjection, pZW37 was linearized using a single cutter restriction enzyme that cuts in the plasmid backbone. Linearized pZW37 was injected at a concentration of 2 ng/uL into both gonadal arms of young adult animals. F1 progeny was picked based on expression of the co-injection marker *unc-122p::gfp* (5 ng/uL) and animals that transmitted the array to F2 progeny were used to generate transgenic lines. Two independent lines (obtained from independent injected P0 animals) were used in subsequent experiments. *ceh-48(syb5859)* and *egl-3(syb5804)* alleles contain an insertion of a *FLAG::NLS::Cre::SL2* cassette before the start codon (generated by SunyBiotech). The 300bp *unc-47* regulatory region was amplified from pMG071 with SpeI and XmaI sites appended. The amplified and cut *unc-47* regulatory region was cloned into a miniMOS vector containing a version of Cre optimized for efficiency in *C. elegans* (Ruijtenberg and van den Heuvel 2015) and a 3' UTR from *unc-54*. Single-copy insertions were generated using the standard miniMOS protocol (Frokjaer-Jensen et al. 2014).

Genetic manipulation of the *pha-4* locus

CRISPR/Cas9 genome editing was carried out to manipulate the *pha-4* locus, using a modified version of a previously established protocol (Eroglu et al. 2023). The injection mixture for all CRISPR experiments consisted of 250 ng/µL of *S. pyogenes* Cas9 nuclease (IDT), 100 ng/µL of tracrRNA (IDT), 56 ng/µL (combined) of all crRNAs (IDT), and 100 ng/µL of each single-stranded oligodeoxynucleotide (ssODN) repair template (IDT). tracrRNA and all crRNAs were heated at 95°C for 5 minutes, followed by cooling to 10°C for 5 minutes. Cas9 was then added to the mix, thoroughly pipetted, and incubated at 25°C for 10 minutes. Next, ssODN and plasmids were incorporated into the mix, and the total volume was brought up to 20 µL with nuclease-free water. The mixture was centrifuged at 17,900 xg for 2 minutes,

and the supernatant was collected for microinjection. A *dpy-10* co-CRISPR strategy was used, employing a crRNA (GCTACCATAGGCACCACGAGGTTTTAGAGCTATGCT) and ssODN (CACTTGAACTTCAATACGGCAAGATGAGAATGACTGGAAACCGTACCGCATGCGGTGCCTATGGTAGCGGAGCTTCACATGGCTTCAGACCAACAGCCTAT). F1 animals were selected based on the roller phenotype, and genotyping was performed by PCR amplification of the edited locus, followed by sequencing via Sanger (Azenta) or Oxford Nanopore (Plasmidsaurus). From confirmed heterozygous F1 plates, non-roller progeny were singled, propagated, and genotyped by PCR to establish homozygous lines.

pha-4(ot946) and *pha-4(ot946 ot1078)* were generated using reagents from IDT, and as previously described (Dokshin et al. 2018). The *pha-4* locus was tagged with *gfp-loxP-3xFLAG* at its 3' end to generate *pha-4(ot946)*. One crRNA (attggagatttataggttgg) and an asymmetric double-stranded gfp-loxP-3xFLAG cassette were used to insert the fluorescent tag at the C-terminal. For *pha-4(ot946 ot1078)*, one crRNA (acataagtgctcattaacag) and a ssODN donor (ccttctgtgtataatagcacataagtgctcattaaATAACTTCGTATAGCATACATTATACGAAGTTATcaggggatactcgatgtcaatatgacccggccagg) were used to insert a second loxP site after *pha-4* first exon (position +278). *pha-4(ot946 ot1078 syb5755)* was further edited (SunyBiotech) with insertion of a GAS flexible linker and the 45 amino acid long Auxin-Inducible Degron (AID) after the GFP located at the C-terminal.

Mutant alleles for *pha-4* (schematized in **Fig.5A**) were generated using two crRNAs and an ssODN donor. The sequences are as follows:

pha-4(ot1505) crRNAs: ACATTATTGATATAAGGGTA and AATTAAACTATTTTGTTTGA
ssODN:CGCCATCCAGTGATGAGGACATTATTGATATAAGGGTCATCAAAGAGGAGCCAGAGTCGGAACCTGACTC

pha-4(ot1506) crRNAs: GTCCACTGCGTATTTTTTGA and TAAAAGGAGAACGTGTGAAT
ssODN:ACCTTATACACCCTATCTGTCCACTGCGTATTTTTCACACGTTCTCCTTTTATTGGAACAGGGCATAGGA.

FLInt-mediated transgene integration

The *otIs946* and *otIs908* transgenes were integrated into the intergenic *oxTi553[eft-3p::tdTomato::H2B::unc-54 3' UTR + Cbr-unc-119(+)] V* locus using the Fluorescent Landmark Interference (FLInt) technique (Malaiwong et al. 2023). To prepare the FLInt injection mixes, tracrRNA (final concentration of 100 ng/µL) and a crRNA (final concentration: 56 ng/µL) targeting the tdTomato locus were combined and incubated at 95°C for 5 minutes, followed by a 5-minute incubation at 10°C. Cas9 (final concentration: 250 ng/µL) was then added, mixed by pipetting, and incubated at 25°C for 10 minutes. Afterward, all plasmids were added at specified concentrations. The final volume was brought to 20 µL using nuclease-free water, followed by centrifugation at 17,900 xg for 2 minutes. The supernatant was then used for microinjections. Injected animals were maintained at room temperature, and F1 progeny expressing the co-injection marker were singled onto separate plates. F2 progeny were selected from F1 plates where at least 75% of the animals expressed the co-injection marker. F2 plates that showed transmission of the co-injection marker in 100% of the progeny were used to establish lines.

Survival Assays

For each genotype, ten age-synchronized L4 stage hermaphrodites were transferred from uncrowded, non-starved plates to ten individual fresh NGM plates seeded with *E. coli* OP50 bacteria. After 24 hours at 20°C, parent worms were transferred to new NGM plates seeded with OP50 bacteria. The number of live larvae and unhatched embryos was counted for each plate after an additional 24 hours at 20°C. Parent worms were iteratively transferred and progeny counted in 24 hour intervals two additional times, and the total hatch rate was pooled for each individual parent.

Pharyngeal pumping assays

All pharyngeal pumping assays were performed on freely moving animals. Age-synchronized adult worms were transferred from uncrowded, non-starved plates to fresh NGM plates seeded with a uniform thin layer of *E. coli* OP50 bacteria. After a 5-minute

acclimatization period, worms were placed under a Nikon Eclipse E400 upright microscope equipped with differential interference contrast (DIC) optics. Before recording behavior, worms were allowed to acclimate to the light source intensity under the microscope for an additional 5 minutes. The movement of the grinder of the pharynx was then recorded with a hand-held tally counter using a 20x air objective lens. The number of grinder movements in 20 seconds was recorded and multiplied by three to obtain pharyngeal pumps per minute. The pharyngeal pumping rate was recorded from at least 8 animals each day and data was pooled from at least on two independent days.

Defecation assays

All defecation assays were performed on freely moving animals. Age-synchronized adult worms were transferred from uncrowded, non-starved plates to fresh NGM plates seeded with a uniform thin layer of *E. coli* OP50 bacteria. After a 5-minute acclimatization period, worms were placed under a Nikon Eclipse E400 upright microscope equipped with DIC optics. Before recording behavior, worms were allowed to acclimate to the light source intensity under the microscope for an additional 5 minutes. Defecation behavior was observed under the 20x air objective lens. Each animal was observed for a 6 min period, during which the timings of contraction of posterior body muscles (pBoc) and expulsion (Exp) muscle contraction that releases food contents from the anal opening were recorded. Defecation behavior was recorded from at least six animals on each day and data was pooled from at least two independent days.

Histamine-mediated chemogenetic silencing of neurons

The inducible silencing of RIS and PVT neurons was conducted using the histamine-gated chloride channel HisCl1 from *Drosophila melanogaster* and by the addition of exogenous histamine as previously described (Pokala et al. 2014). Histamine dihydrochloride (Sigma-Aldrich H7250) was dissolved in water to prepare 1M stock solutions. NGM Agar containing 0 mM (control), 8 mM, and 10 mM histamine dihydrochloride was added to 60mm plates. Age-synchronized adults were transferred to NGM agar control and histamine plates immediately prior to experiments. After a recovery period, worms were observed for pharyngeal pumping and defecation behavior under a Nikon Eclipse E400 upright microscope

equipped with DIC optics. For L1 molting experiments, worms were age-synchronized in the L1 stage and observed for pharyngeal pumping and defecation behavior 9 hours after being added to NGM control and histamine plates at 23°C.

5-Ph-IAA treatment for AID2

AID-tagged proteins are conditionally degraded when exposed to 5-Ph-IAA in the presence of TIR1(F79G). All AID2 experiments were carried out as described previously with some modifications (Sural et al. 2024). To generate the experimental strain, the conditional allele *pha-4(ot946 ot1078 syb5755)* was crossed with *otIs908* which expresses TIR1(F79G) in all neurons of the pharyngeal nervous system and AVL, RIS, and DVB. The synthetic auxin analog 5-Ph-IAA was acquired from BioAcademia (#30- 003-10) and dissolved in ethanol (EtOH) to prepare 100 mM stock solutions. NGM agar plates seeded with a uniform lawn of *E. coli* OP50 bacteria were coated with 100 µL of freshly prepared 5-Ph-IAA stock solution and allowed to dry and diffuse overnight at room temperature to final concentrations of 100 µM and 200 µM. Age-synchronized embryos (obtained via the alkaline bleaching method), L1s, or L4s were transferred to the plates one day after adding 5-Ph-IAA, and the animals were grown at 24°C for an additional 24 hours until they reached the desired developmental stage for the experiment. In control conditions, worms were transferred onto EtOH-coated plates. All plates were shielded from light for the duration of the experiment to limit degradation of 5-Ph-IAA.

Heat shock

Young adult worms were picked onto fresh NGM plates (5 worms per plate) and incubated at 15°C. After 24 hours, adult worms were removed, leaving developing progeny. The next day, worms were subjected to heat shock at 37°C for three 30-minute intervals, with 1 hour recovery at 20°C between each heat shock. After heat shock, worms were maintained at 25°C until pharyngeal pumping assays were performed.

Microscopy

Worms were anesthetized using 100 mM sodium azide (NaN_3) and mounted on 5% agarose pads on glass slides. Animals were imaged on an inverted Zeiss LSM 980 laser scanning confocal microscope using a 40x water immersion objective lens, or a Zeiss Imager Z2 upright microscope equipped with Colibri 7 LEDs (Zeiss) using a 40x oil immersion objective lens. For each image, Z-stacks of uniform 0.31 µm - 1 µm thickness (depending on age of the worm) were obtained for the entire sample.

Reporter gene expression in different neurons was visualized in wild-type and mutant animals and usually assigned to one of the following categories: ‘on’ (fluorescence levels comparable to wild- type animals), ‘dim’ (fluorescence still detectable but much dimmer than wild-type animals), or ‘off’ (fluorescence not detectable) by the observer.

Statistical analysis

All images were processed and analyzed using ImageJ FIJI (Schindelin et al. 2012). All plotting and statistical tests were performed on GraphPad Prism 10. Sample sizes for pharyngeal pumping and defecation assays are a minimum of 32 and 12 animals respectively, based on standards established in prior studies using these behavioral readouts. These sample sizes have been shown to reliably detect physiologically relevant differences. For microscopy images, a minimum of 8 animals were imaged per condition, and a representative image is shown. The figure legends include the statistical tests applied in each figure along with the corresponding P values. $P < 0.05$ was considered to be statistically significant.

COMPETING INTEREST STATEMENT

The authors declare that they have no competing interests.

ACKNOWLEDGEMENT

We thank Qi Chen for expert help in generating transgenic strains, and Rudy LeDuc, Emma Grungold and Tristian Wiles for their involvement in generating the *unc-47prom::cre* line. Some strains were provided by the CGC, which is funded by NIH Office of Research Infrastructure Programs (P40 OD010440). This work was funded, in part, by the NIH (R01 NS039996) and the Howard Hughes Medical Institute.

AUTHOR CONTRIBUTIONS

Conceptualization: OH
Methodology: ZW, WXC, ELD, MR, SS, MAA
Investigation: ZW, WXC, ELD, MR, SS, MAA
Visualization: ZW, WXC, SS
Supervision: OH
Writing—original draft: OH
Writing—review & editing: ZW, WXC, ELD, MR, SS, MAA, OH

REFERENCES

Adler CE, Seidel CW, McKinney SA, Sanchez Alvarado A. 2014. Selective amputation of the pharynx identifies a FoxA-dependent regeneration program in planaria. *eLife* **3**: e02238.

Albertson DG, Thomson JN. 1976. The pharynx of Caenorhabditis elegans. *Philos Trans R Soc Lond B Biol Sci* **275**: 299-325.

Annunziata R, Andrikou C, Perillo M, Cuomo C, Arnone MI. 2019. Development and evolution of gut structures: from molecules to function. *Cell Tissue Res* **377**: 445-458.

Ao W, Gaudet J, Kent WJ, Muttumu S, Mango SE. 2004. Environmentally induced foregut remodeling by PHA-4/FoxA and DAF-12/NHR. *Science* **305**: 1743-1746.

Aurelio O, Boulin T, Hobert O. 2003. Identification of spatial and temporal cues that regulate postembryonic expression of axon maintenance factors in the C. elegans ventral nerve cord. *Development* **130**: 599-610.

Avery L, Horvitz HR. 1989. Pharyngeal pumping continues after laser killing of the pharyngeal nervous system of C. elegans. *Neuron* **3**: 473-485.

Avery L, Thomas JH. 1997. Feeding and Defecation. in *Celegans II* (eds. DL Riddle, T Blumenthal, BJ Meyer, JR Priess), pp. 679-716. Cold Spring Harbor Laboratory Press.

Azzaria M, Goszczynski B, Chung MA, Kalb JM, McGhee JD. 1996. A fork head/HNF-3 homolog expressed in the pharynx and intestine of the Caenorhabditis elegans embryo. *Dev Biol* **178**: 289-303.

Cao WX, Merritt DM, Pe K, Cesar M, Hobert O. 2024. Comparative analysis of new mScarlet-based red fluorescent tags in Caenorhabditis elegans. *Genetics* **228**.

Chen D, Riddle DL. 2008. Function of the PHA-4/FOXA transcription factor during C. elegans post-embryonic development. *BMC Dev Biol* **8**: 26.

Choi U, Wang H, Hu M, Kim S, Sieburth D. 2021. Presynaptic coupling by electrical synapses coordinates a rhythmic behavior by synchronizing the activities of a neuron pair. *Proc Natl Acad Sci U S A* **118**.

Cook SJ, Crouse CM, Yemini E, Hall DH, Emmons SW, Hobert O. 2020. The connectome of the Caenorhabditis elegans pharynx. *The Journal of comparative neurology*.

Dal Santo P, Logan MA, Chisholm AD, Jorgensen EM. 1999. The inositol trisphosphate receptor regulates a 50-second behavioral rhythm in C. elegans. *Cell* **98**: 757-767.

Dokshin GA, Ghanta KS, Piscopo KM, Mello CC. 2018. Robust Genome Editing with Short Single-Stranded and Long, Partially Single-Stranded DNA Donors in Caenorhabditis elegans. *Genetics* **210**: 781-787.

Eroglu M, Yu B, Derry WB. 2023. Efficient CRISPR/Cas9 mediated large insertions using long single-stranded oligonucleotide donors in C. elegans. *The FEBS journal*.

Fakhouri TH, Stevenson J, Chisholm AD, Mango SE. 2010. Dynamic chromatin organization during foregut development mediated by the organ selector gene PHA-4/FoxA. *PLoS Genet* **6**.

Friedman JR, Kaestner KH. 2006. The Foxa family of transcription factors in development and metabolism. *Cell Mol Life Sci* **63**: 2317-2328.

Frokjaer-Jensen C, Davis MW, Sarov M, Taylor J, Flibotte S, LaBella M, Pozniakovsky A, Moerman DG, Jorgensen EM. 2014. Random and targeted transgene insertion in Caenorhabditis elegans using a modified Mos1 transposon. *Nat Methods* **11**: 529-534.

Furness JB. 2012. The enteric nervous system and neurogastroenterology. *Nat Rev Gastroenterol Hepatol* **9**: 286-294.

Furness JB, Stebbing MJ. 2018. The first brain: Species comparisons and evolutionary implications for the enteric and central nervous systems. *Neurogastroenterol Motil* **30**.
Gaudet J, Mango SE. 2002. Regulation of organogenesis by the Caenorhabditis elegans FoxA protein PHA-4. *Science* **295**: 821-825.
Gaudet J, Muttumu S, Horner M, Mango SE. 2004. Whole-genome analysis of temporal gene expression during foregut development. *PLoS Biol* **2**: e352.
Gendrel M, Atlas EG, Hobert O. 2016. A cellular and regulatory map of the GABAergic nervous system of C. elegans. *eLife* **5**.
Gershon MD. 1998. *The Second Brain*. HarperCollins.
Gerstein MB Lu ZJ Van Nostrand EL Cheng C Arshinoff BI Liu T Yip KY Robilotto R Rechtsteiner A Ikegami K et al. 2010. Integrative analysis of the Caenorhabditis elegans genome by the modENCODE project. *Science* **330**: 1775-1787.
Grosshans H, Johnson T, Reinert KL, Gerstein M, Slack FJ. 2005. The temporal patterning microRNA let-7 regulates several transcription factors at the larval to adult transition in C. elegans. *Dev Cell* **8**: 321-330.
Grubbs JJ, Lopes LE, van der Linden AM, Raizen DM. 2020. A salt-induced kinase is required for the metabolic regulation of sleep. *PLoS Biol* **18**: e3000220.
Hall DH, Altun Z. 2007. *C. Elegans Atlas*. Cold Spring Harbor Laboratory Press.
Hartenstein V. 1997. Development of the insect stomatogastric nervous system. *Trends in neurosciences* **20**: 421-427.
Hills-Muckey K, Martinez MAQ, Stec N, Hebbar S, Saldanha J, Medwig-Kinney TN, Moore FEQ, Ivanova M, Morao A, Ward JD et al. 2022. An engineered, orthogonal auxin analog/AtTIR1(F79G) pairing improves both specificity and efficacy of the auxin degradation system in Caenorhabditis elegans. *Genetics* **220**.
Hobert O, Tessmar K, Ruvkun G. 1999. The Caenorhabditis elegans lim-6 LIM homeobox gene regulates neurite outgrowth and function of particular GABAergic neurons. *Development* **126**: 1547-1562.
Horner MA, Quintin S, Domeier ME, Kimble J, Labouesse M, Mango SE. 1998. pha-4, an HNF-3 homolog, specifies pharyngeal organ identity in Caenorhabditis elegans. *Genes Dev* **12**: 1947-1952.
Hsu HT, Chen HM, Yang Z, Wang J, Lee NK, Burger A, Zaret K, Liu T, Levine E, Mango SE. 2015. TRANSCRIPTION. Recruitment of RNA polymerase II by the pioneer transcription factor PHA-4. *Science* **348**: 1372-1376.
Jiang J, Su Y, Zhang R, Li H, Tao L, Liu Q. 2022. C. elegans enteric motor neurons fire synchronized action potentials underlying the defecation motor program. *Nat Commun* **13**: 2783.
Kalb JM, Lau KK, Goszczynski B, Fukushige T, Moons D, Okkema PG, McGhee JD. 1998. pha-4 is Ce-fkh-1, a fork head/HNF-3alpha,beta,gamma homolog that functions in organogenesis of the C. elegans pharynx. *Development* **125**: 2171-2180.
Kaltenbach LS, Updike DL, Mango SE. 2005. Contribution of the amino and carboxyl termini for PHA-4/FoxA function in Caenorhabditis elegans. *Dev Dyn* **234**: 346-354.
Kim K, Li C. 2004. Expression and regulation of an FMRFamide-related neuropeptide gene family in Caenorhabditis elegans. *The Journal of comparative neurology* **475**: 540-550.
Laranjeira C, Pachnis V. 2009. Enteric nervous system development: Recent progress and future challenges. *Auton Neurosci* **151**: 61-69.
Leyva-Diaz E, Hobert O. 2022. Robust regulatory architecture of pan-neuronal gene expression. *Curr Biol* **32**: 1715–1727.

Ma X, Zhao Z, Xiao L, Xu W, Kou Y, Zhang Y, Wu G, Wang Y, Du Z. 2021. A 4D single-cell protein atlas of transcription factors delineates spatiotemporal patterning during embryogenesis. *Nat Methods* **18**: 893-902.
Mahoney TR, Luo S, Round EK, Brauner M, Gottschalk A, Thomas JH, Nonet ML. 2008. Intestinal signaling to GABAergic neurons regulates a rhythmic behavior in Caenorhabditis elegans. *Proc Natl Acad Sci U S A* **105**: 16350-16355.
Malaiwong N, Porta-de-la-Riva M, Krieg M. 2023. FLInt: single shot safe harbor transgene integration via Fluorescent Landmark Interference. *G3 (Bethesda)* **13**.
Mango SE. 2009. The molecular basis of organ formation: insights from the C. elegans foregut. *Annu Rev Cell Dev Biol* **25**: 597-628.
Mango SE, Lambie EJ, Kimble J. 1994. The pha-4 gene is required to generate the pharyngeal primordium of Caenorhabditis elegans. *Development* **120**: 3019-3031.
Marquina-Solis J, Feng L, Vandewyer E, Beets I, Hawk J, Colon-Ramos DA, Yu J, Fox BW, Schroeder FC, Bargmann CI. 2024. Antagonism between neuropeptides and monoamines in a distributed circuit for pathogen avoidance. *Cell Rep* **43**: 114042.
McIntire SL, Jorgensen E, Kaplan J, Horvitz HR. 1993. The GABAergic nervous system of Caenorhabditis elegans. *Nature* **364**: 337-341.
McIntire SL, Reimer RJ, Schuske K, Edwards RH, Jorgensen EM. 1997. Identification and characterization of the vesicular GABA transporter. *Nature* **389**: 870-876.
McKay SJ, Johnsen R, Khattra J, Asano J, Baillie DL, Chan S, Dube N, Fang L, Goszczynski B, Ha E et al. 2003. Gene expression profiling of cells, tissues, and developmental stages of the nematode C. elegans. *Cold Spring Harb Symp Quant Biol* **68**: 159-169.
Nagy N, Goldstein AM. 2017. Enteric nervous system development: A crest cell's journey from neural tube to colon. *Semin Cell Dev Biol* **66**: 94-106.
Niu L, Li Y, Zong P, Liu P, Shui Y, Chen B, Wang ZW. 2020. Melatonin promotes sleep by activating the BK channel in C. elegans. *Proc Natl Acad Sci U S A* **117**: 25128-25137.
Niu W, Lu ZJ, Zhong M, Sarov M, Murray JI, Brdlik CM, Janette J, Chen C, Alves P, Preston E et al. 2011. Diverse transcription factor binding features revealed by genome-wide ChIP-seq in C. elegans. *Genome Res* **21**: 245-254.
Panowski SH, Wolff S, Aguilaniu H, Durieux J, Dillin A. 2007. PHA-4/Foxa mediates diet-restriction-induced longevity of C. elegans. *Nature* **447**: 550-555.
Pereira L, Aeschimann F, Wang C, Lawson H, Serrano-Saiz E, Portman DS, Grosshans H, Hobert O. 2019. Timing mechanism of sexually dimorphic nervous system differentiation. *eLife* **8**.
Pokala N, Liu Q, Gordus A, Bargmann CI. 2014. Inducible and titratable silencing of Caenorhabditis elegans neurons in vivo with histamine-gated chloride channels. *Proc Natl Acad Sci U S A* **111**: 2770-2775.
Rao M, Gershon MD. 2018. Enteric nervous system development: what could possibly go wrong? *Nat Rev Neurosci* **19**: 552-565.
Riddle MR, Spickard EA, Jevince A, Nguyen KC, Hall DH, Joshi PM, Rothman JH. 2016. Transorganogenesis and transdifferentiation in C. elegans are dependent on differentiated cell identity. *Dev Biol* **420**: 136-147.
Ripoll-Sanchez L, Watteyne J, Sun H, Fernandez R, Taylor SR, Weinreb A, Bentley BL, Hammarlund M, Miller DM, 3rd, Hobert O et al. 2023. The neuropeptidergic connectome of C. elegans. *Neuron* **111**: 3570-3589 e3575.
Ruijtenberg S, van den Heuvel S. 2015. G1/S Inhibitors and the SWI/SNF Complex Control Cell-Cycle Exit during Muscle Differentiation. *Cell* **162**: 300-313.

Sarov M, Schneider S, Pozniakovski A, Roguev A, Ernst S, Zhang Y, Hyman AA, Stewart AF. 2006. A recombineering pipeline for functional genomics applied to Caenorhabditis elegans. *Nat Methods* **3**: 839-844.
Sasselli V, Pachnis V, Burns AJ. 2012. The enteric nervous system. *Dev Biol* **366**: 64-73.
Schindelin J, Arganda-Carreras I, Frise E, Kaynig V, Longair M, Pietzsch T, Preibisch S, Rueden C, Saalfeld S, Schmid B et al. 2012. Fiji: an open-source platform for biological-image analysis. *Nat Methods* **9**: 676-682.
Serrano-Saiz E, Pereira L, Gendrel M, Aghayeva U, Battacharya A, Howell K, Garcia LR, Hobert O. 2017. A Neurotransmitter Atlas of the Caenorhabditis elegans Male Nervous System Reveals Sexually Dimorphic Neurotransmitter Usage. *Genetics* **206**: 1251-1269.
Serrano-Saiz E, Poole Richard J, Felton T, Zhang F, De La Cruz Estanisla D, Hobert O. 2013. Modular Control of Glutamatergic Neuronal Identity in C. elegans by Distinct Homeodomain Proteins. *Cell* **155**: 659-673.
Steuer Costa W, Van der Auwera P, Glock C, Liewald JF, Bach M, Schuler C, Wabnig S, Oranth A, Masurat F, Bringmann H et al. 2019. A GABAergic and peptidergic sleep neuron as a locomotion stop neuron with compartmentalized Ca2+ dynamics. *Nat Commun* **10**: 4095.
Sun H, Beets I, Schafer W, Hobert O. 2023. Comparing engineered nuclear-localized reporter cassettes. *MicroPubl Biol* **2023**.
Sural S, Botero JQ, Hobert O, Tekle-Smith M. 2024. Protocol to synthesize the auxin analog 5-Ph-IAA for conditional protein depletion in C. elegans using the AID2 system. *STAR Protoc* **5**: 102901.
Sural S, Walker Z, Hobert O. 2025. Gut epithelium modifies enteric behaviors during nutritional adversity via distinct peptidergic signaling axes. *BioRxiv*.
Taylor SR, Santpere G, Weinreb A, Barrett A, Reilly MB, Xu C, Varol E, Oikonomou P, Glenwinkel L, McWhirter R et al. 2021. Molecular topography of an entire nervous system. *Cell* **184**: 4329-4347 e4323.
Thomas JH. 1990. Genetic analysis of defecation in Caenorhabditis elegans. *Genetics* **124**: 855-872.
Torzone SK, Park AY, Breen PC, Cohen NR, Dowen RH. 2023. Opposing action of the FLR-2 glycoprotein hormone and DRL-1/FLR-4 MAP kinases balance p38-mediated growth and lipid homeostasis in C. elegans. *PLoS Biol* **21**: e3002320.
Updike DL, Mango SE. 2007. Genetic suppressors of Caenorhabditis elegans pha-4/FoxA identify the predicted AAA helicase ruvb-1/RuvB. *Genetics* **177**: 819-833.
Vidal B, Gulez B, Cao WX, Leyva-Diaz E, Reilly MB, Tekieli T, Hobert O. 2022. The enteric nervous system of the C. elegans pharynx is specified by the Sine oculis-like homeobox gene ceh-34. *eLife* **11**.
Wang C, Vidal B, Sural S, Loer C, Aguilar GR, Merritt DM, Toker IA, Vogt MC, Cros CC, Hobert O. 2024. A neurotransmitter atlas of C. elegans males and hermaphrodites. *eLife* **13**.
Wang H, Girskis K, Janssen T, Chan JP, Dasgupta K, Knowles JA, Schoofs L, Sieburth D. 2013. Neuropeptide secreted from a pacemaker activates neurons to control a rhythmic behavior. *Curr Biol* **23**: 746-754.
Wu J, Jiang X, Li Y, Zhu T, Zhang J, Zhang Z, Zhang L, Zhang Y, Wang Y, Zou X et al. 2018. PHA-4/FoxA senses nucleolar stress to regulate lipid accumulation in Caenorhabditis elegans. *Nat Commun* **9**: 1195.

Yemini E, Lin A, Nejatbakhsh A, Varol E, Sun R, Mena GE, Samuel ADT, Paninski L, Venkatachalam V, Hobert O. 2021. NeuroPAL: A Multicolor Atlas for Whole-Brain Neuronal Identification in C. elegans. *Cell* **184**: 272-288 e211.

Zaret KS, Carroll JS. 2011. Pioneer transcription factors: establishing competence for gene expression. *Genes Dev* **25**: 2227-2241.

Zhang L, Ward JD, Cheng Z, Dernburg AF. 2015. The auxin-inducible degradation (AID) system enables versatile conditional protein depletion in C. elegans. *Development* **142**: 4374-4384.

FIGURES

FIGURE 1

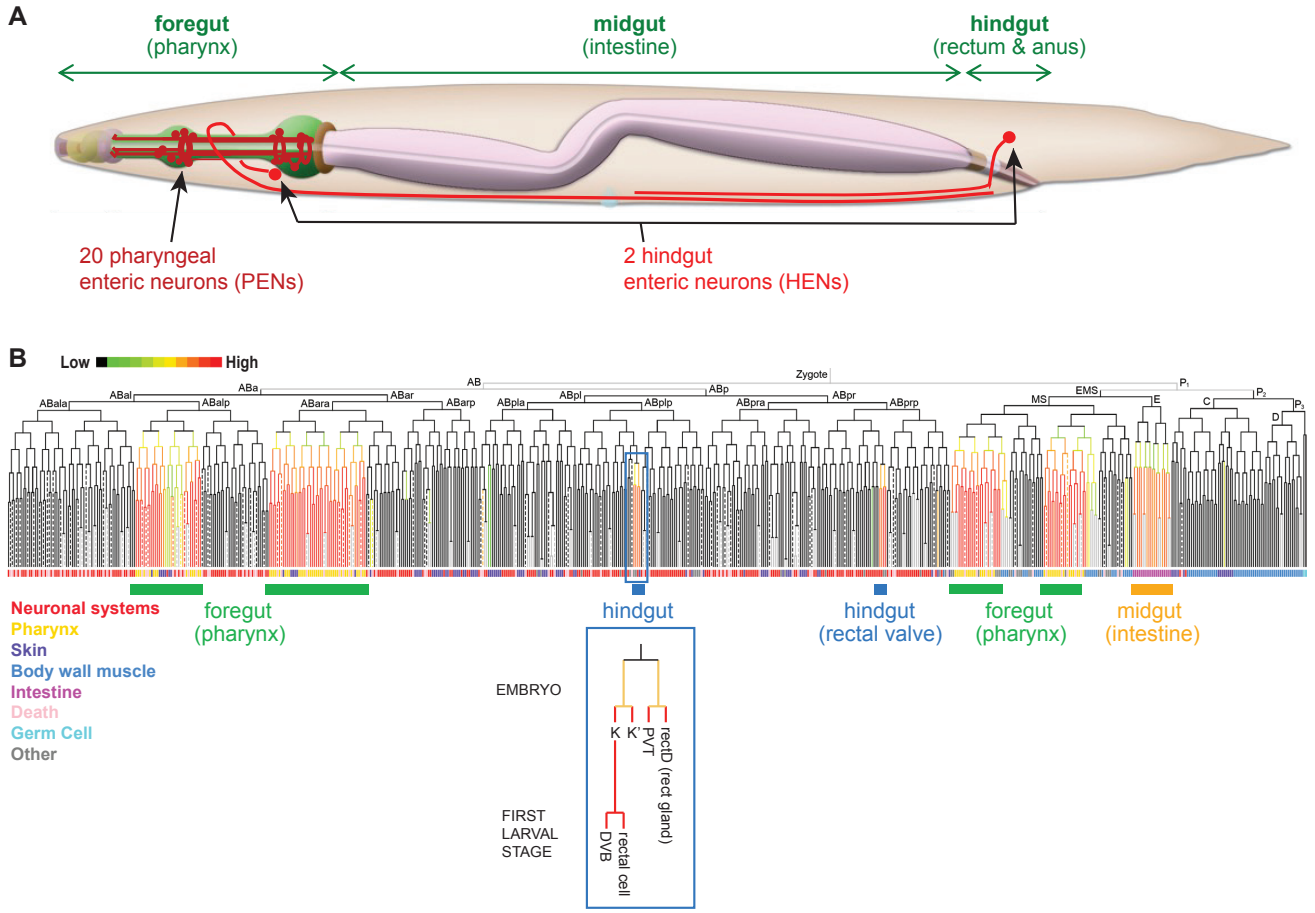

C

Cell Type	Lineage	Expression prev. described *	Reporter allele expression **	Δ Expression
Alimentary tract				
Arcade cells	AB	Embryo, Larva, Adult	Embryo, Larva, Adult	No change
Pharyngeal epithelial cells	AB	Embryo, Larva, Adult	Embryo, Larva, Adult	No change
Pharyngeal marginal cells	AB	Embryo, Larva, Adult	Embryo, Larva, Adult	No change
Pharyngeal gland cells	MS	Embryo, Larva, Adult	Embryo, Larva, Adult	No change
Pharyngeal muscle cells	AB/MS	Embryo, Larva, Adult	Embryo, Larva, Adult	No change
Pharyngeal neurons	AB/MS	Embryo, Larva, Adult	Embryo, Larva, Adult	Decreases
Pharyngeal intestinal valve	MS	Embryo, Larva, Adult	Embryo, Larva, Adult	No change
Intestinal Cells	E	Embryo, Larva, Adult	Embryo, Larva, Adult	Decreases
Intestinal-Rectal valve cells	AB	Embryo, Larva, Adult	Embryo, Larva, Adult	No change
Rectal gland cell	AB	Embryo, Larva, Adult	Embryo, Larva, Adult	No change
Rectal Epithelial Cells	AB	Embryo, Larva, Adult	Embryo, Larva, Adult	No change
Ventral ganglion - AVL	AB	no ("head neuron in adult")	Embryo, Larva, Adult	No change
Ventral ganglion - RIS	AB	no	Embryo, Larva, Adult	No change
Pre-anal ganglion - PVT	AB	no	Larva, Adult	No change
Rectal Neurons - DVB	K	no ("tail neuron in adult")	Post - L1	Post- L1
Outside Alimentary tract				
Anterior distal tip cells	Z1	Larva	L2 - L4 stage	L2 - L4 stage
Posterior distal tip cells	Z4	Larva	L2 - L4 stage	L2 - L4 stage
Uterine epithelial cells	Z1/Z4	Larva	L3-L4 stage	L3-L4 stage
Uterine vulval cells	P	Larva	L3-L4 stage	L3-L4 stage

Figure 1: The *C. elegans* alimentary system, enteric neurons and PHA-4 expression.

A: Schematic overview of enteric system, including schematics of the pharyngeal and hindgut enteric neurons Adapted from *WormAtlas* (Altun, Z.F. and Hall, D.H. 2009.).

B: Embryonic expression of PHA-4 as determined by 4D microscopy of a *pha-4* fosmid-based reporter (Ma et al. 2021). The lineage that generates PVT is highlighted to show its relation to hindgut cells (gland, hindgut-innervating DVB, rectal epithelial cells).

C: Summary of previously reported and new expression pattern of PHA-4. * identified in previous studies using antibody staining and/or reporter transgenes (Horner et al. 1998; Kalb et al. 1998; McKay et al. 2003; Grosshans et al. 2005; Panowski et al. 2007; Chen and Riddle 2008; Riddle et al. 2016) ; ** this paper. "Δ Expression" refers to expression changes observed through stages of animal development. Newly defined sites of expression are in red.

FIGURE 2

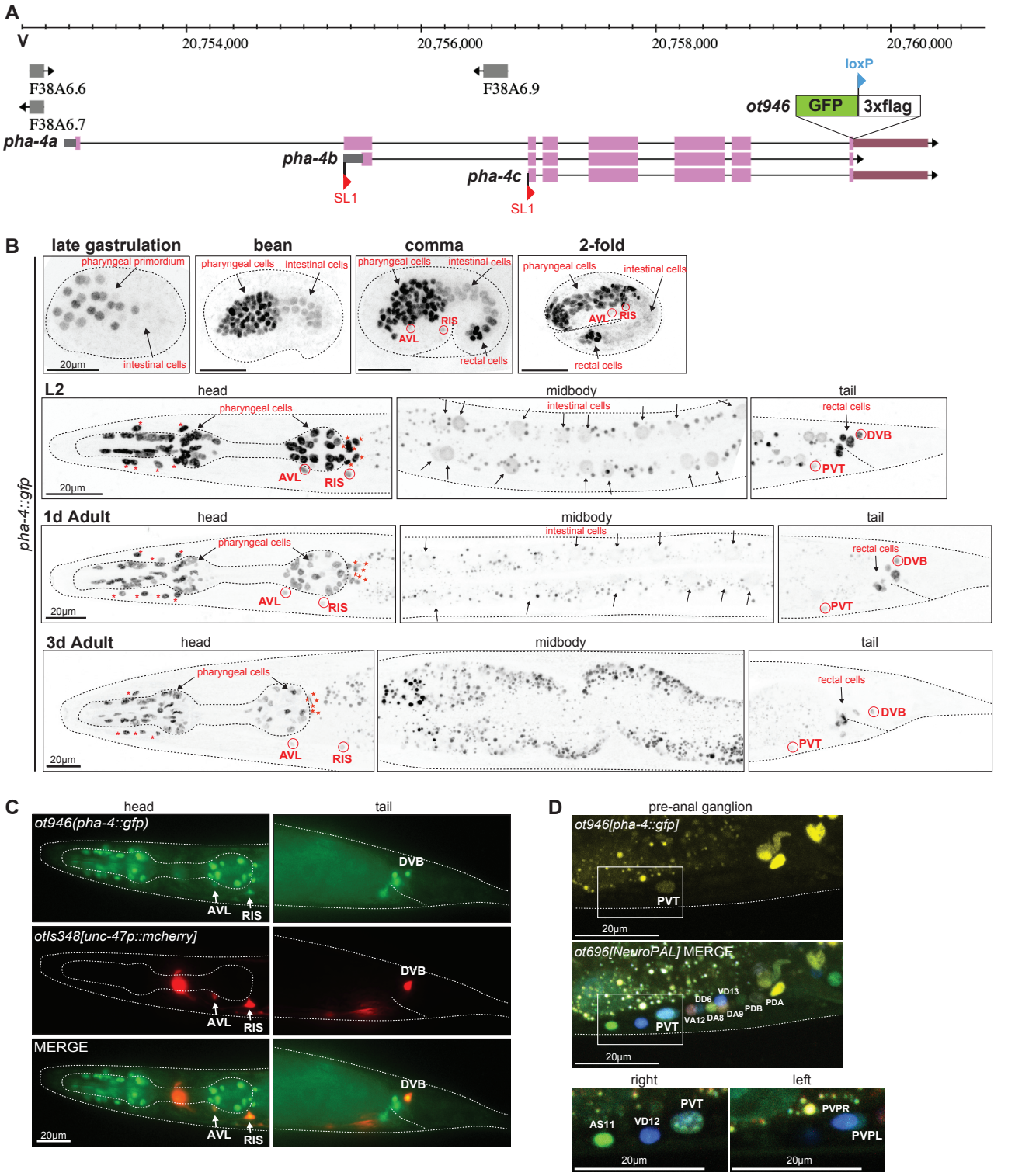

Figure 2: Expression pattern of a *gfp*-tagged *pha-4* locus

A: *pha-4* locus schematic on Chromosome V, showing the *pha-4* CRISPR/Cas-9-engineered reporter allele *ot946*. The different isoforms were inferred from the identification of SL1-trans-spliced transcript (Azzaria et al. 1996).

B: Expression of the *ot946* allele over the course of development, showing expression in the enteric system throughout. Asterisks indicate the arcade cells. Stars indicate the pharyngeal-intestinal valve cells. Overlays with a pan-neuronal reporter are shown in **Fig.S1A**.
C: *pha-4* is expressed in GABAergic neurons AVL, RIS, and DVB. Images of an adult worm show co-localization of *pha-4* expression (*ot946*) with a *unc-47* promoter fusion (*otIs348*) in two neurons situated on the ventral ganglion in the head (AVL and RIS), and one neuron on the dorsal side in the tail (DVB).
D: *pha-4* is expressed in the pre-anal ganglion neuron PVT. Magnified images of the pre-anal ganglion of an adult worm show co-localization of *pha-4* expression (*ot946*) with PVT as identified by NeuroPAL (*otIs696).* NeuroPAL cell IDs of neighboring neurons are also annotated.

FIGURE 3

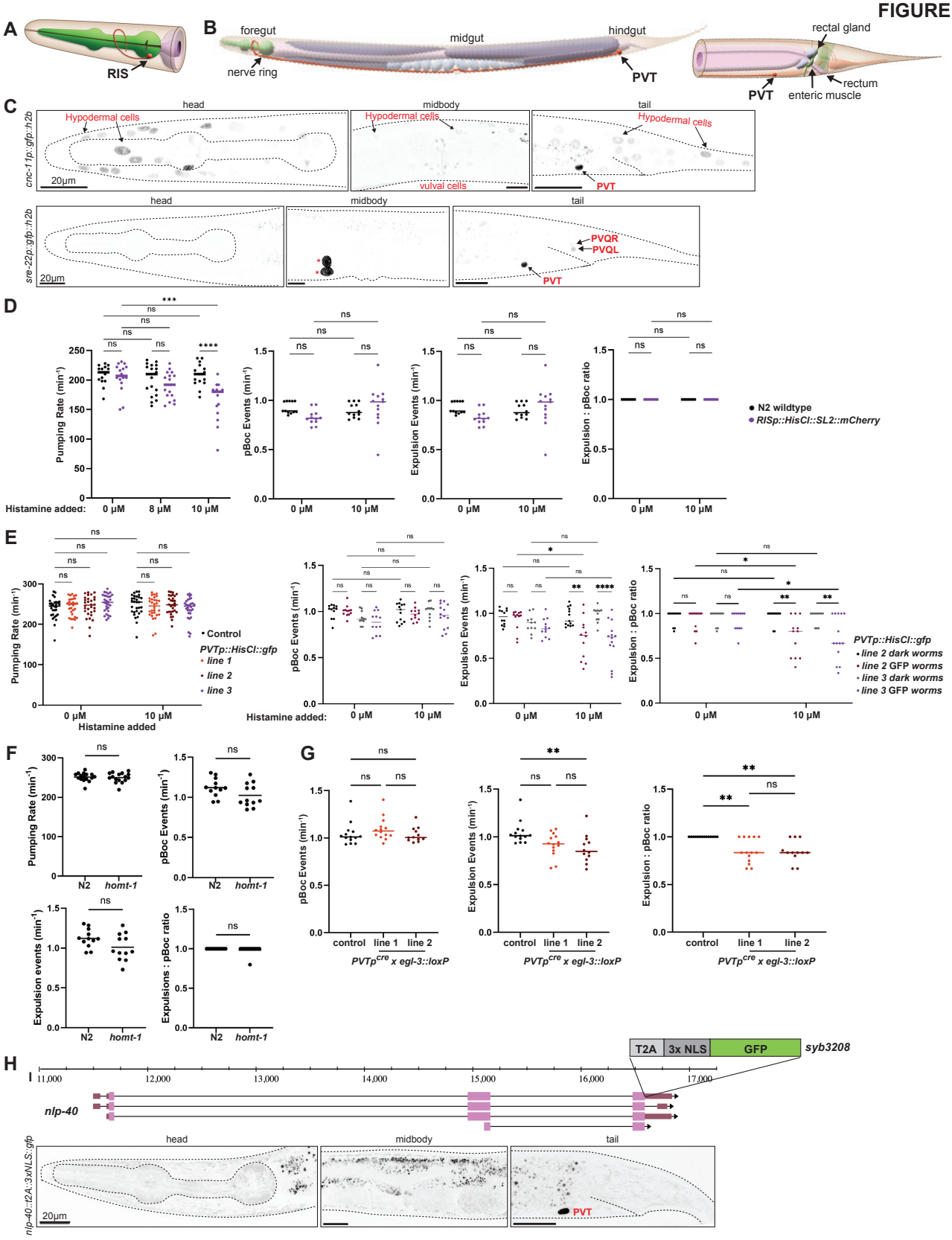
A
RIS
B
foregut
nerve ring
midgut
hindgut
PVT
rectal gland
PVT
enteric muscle
rectum
C
head
midbody
tail
cnc-11p::gfp::h2b
Hypodermal cells
vulval cells
PVT
20µm
sre-22p::gfp::h2b
PVQR
PVQL
D
Pumping Rate (min⁻¹)
pBoc Events (min⁻¹)
Expulsion Events (min⁻¹)
Expulsion : pBoc ratio
Histamine added:
0 µM
8 µM
10 µM
N2 wildtype
RISp::HisCl::SL2::mCherry
E
Control
PVTp::HisCl::gfp
line 1
line 2
line 3
Histamine added
PVTp::HisCl::gfp
line 2 dark worms
line 2 GFP worms
line 3 dark worms
line 3 GFP worms
F
N2
homt-1
Expulsion events (min⁻¹)
Expulsions : pBoc ratio
G
control
line 1
line 2
PVTp^cre x egl-3::loxP
H
T2A
3x NLS
GFP
syb3208
I
nlp-40
nlp-40::t2A::3xNLS::gfp

Figure 3: Effect of RIS and PVT inhibition on enteric behaviors

A: Schematic showing the anatomical location and morphology of the RIS neuron, adapted from *WormAtlas* at www.wormatlas.org (Hall and Altun 2007).

B: Schematics showing the anatomical location and morphology of the PVT neuron, adapted from *WormAtlas* at www.wormatlas.org (Hall and Altun 2007).

C: Establishing cre-driver lines with PVT specificity. Representative images of animals assayed in the day 1 adult stage. Expression of a *cnc-11* promoter fusion (*otEx8345*) (TOP), and *sre-22* promoter fusion *(otEx8333)* (BOTTOM) in the head, midbody, and tail. Expression in PVT and a few other cell types are annotated. Asterisks indicate the expression of the co-injection marker *unc-122p::gfp* in coelomocytes. Expression was confirmed in 14 array positive animals of *sre-22* promoter fusion, and 25 array positive animals of *cnc-11* promoter fusion.

D. Histamine-mediated silencing of RIS impacts adult pumping, but not defecation behavior. Pharyngeal pumping in RIS::HisCl expressing worms (*qnEx643*). Pharyngeal pumping was observed in the absence of histamine (0 μM), and at 8 μM and 10 μM concentrations of histamine. Frequency of pBocs, frequency of expulsion, and the Expulsion : pBoc ratio in RIS::HisCl expressing adult worms treated with histamine were assayed and individually plotted.

E: Histamine-mediated silencing of PVT impacts defecation, but not pharyngeal pumping behavior. Three PVTp::HisCl array-expressing lines (*otEx8336 otEx8337 otEx8338*) were assayed. Behavior was observed at 0 μM, 8 μM, and 10 μM concentrations of histamine. Dark worms are non-array carrying siblings from the PVTp::HisCl lines. Pharyngeal pumping of adult worms from two lines expressing PVTp::HisCl *(otEx8336* and *otEx8337)* treated with histamine. Frequency of pBocs, frequency of expulsion, and expulsion : pBoc ratio in adult worms of two lines expressing PVTp::HisCl *(otEx8336* and *otEx8337*) treated with histamine were assayed and individually plotted.

F: Enteric behaviors are unaffected in the *homt-1* null (*zw94*). Pharyngeal pumping in *homt-1* (*zw94*) adult worms. Frequency of pBocs frequency of expulsion, and expulsion : pBoc ratio in homt-1(*zw94*) adult worms are individually plotted.

G: Cre-mediated removal of *egl-3* from PVT impacts adult defecation. Dark worms are non-array carrying siblings from the *PVTp::Cre egl-3::loxP* lines (*otEx8339* and *otEx8340*). Frequency of pBocs, frequency of expulsion, and expulsion : pBoc ratio in adult worms of two

lines where *egl-3* expression is removed via PVTp::Cre (*otEx8339* and *otEx8340*) are individually plotted.

H: *nlp-40* locus schematic on Chromosome I, showing the *nlp-40* CRISPR/Cas-9-engineered reporter allele *syb3208*. The *T2A::3xNLS::GFP* cassette may result in expression of *nlp-40* in intestinal cells below detectable levels. Below: expression pattern of *nlp-40* across the head, midbody, and tail of an adult worm. Expression is observed only in the PVT neuron.

(**D - G**): Data points show individual worms assayed. Horizontal line represents median value of biological replicates*, **, ***, **** and ns represent $P < 0.05$, $P < 0.007$, $P < 0.001$, $P < 0.0001$ and not significant, respectively, in a Mann-Whitney test (F), and Dunn's multiple comparison test after Kruskal-Wallis test (G), and Sidak's multiple comparisons test after two-way ANOVA (D and E).

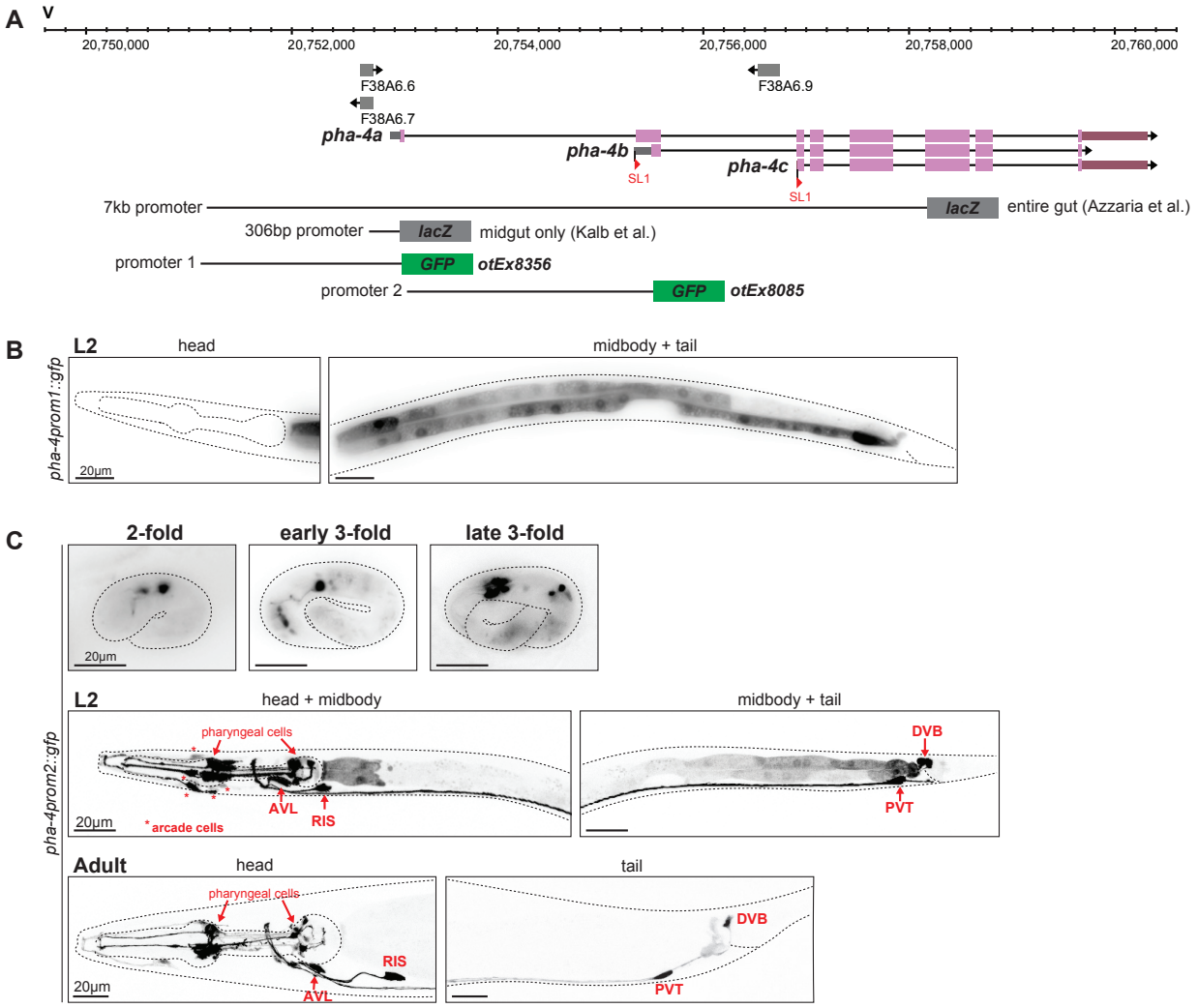

Figure 4: An intronic cis-regulatory element drives PHA-4 expression in PENs and HENs

A: *pha-4* locus schematic with indicated reporter gene fusions. Previously described lacZ fusions from (Azzaria et al. 1996; Kalb et al. 1998) are schematized along with two newly generated promoter fragments fused to GFP and used for expression analyses.

B: Expression pattern of a *pha-4prom1::gfp* reporter (*otEx8356*). An approximately 2kb fragment upstream of the start codon of the *pha-4a* isoform drives expression specifically in the intestinal cells.

C: Expression pattern of a *pha-4prom2::gfp* reporter (*otEx8085*). An approximately 2.4kb fragment upstream of the start codon of *pha-4b* isoform and containing the first intron of *pha-4a,* drives expression specifically in all enteric neurons of the pharynx, hindgut, as well as

RIS and PVT. The onset of GFP expression is detected in the embryo, and expression is maintained through to adulthood.

FIGURE 5

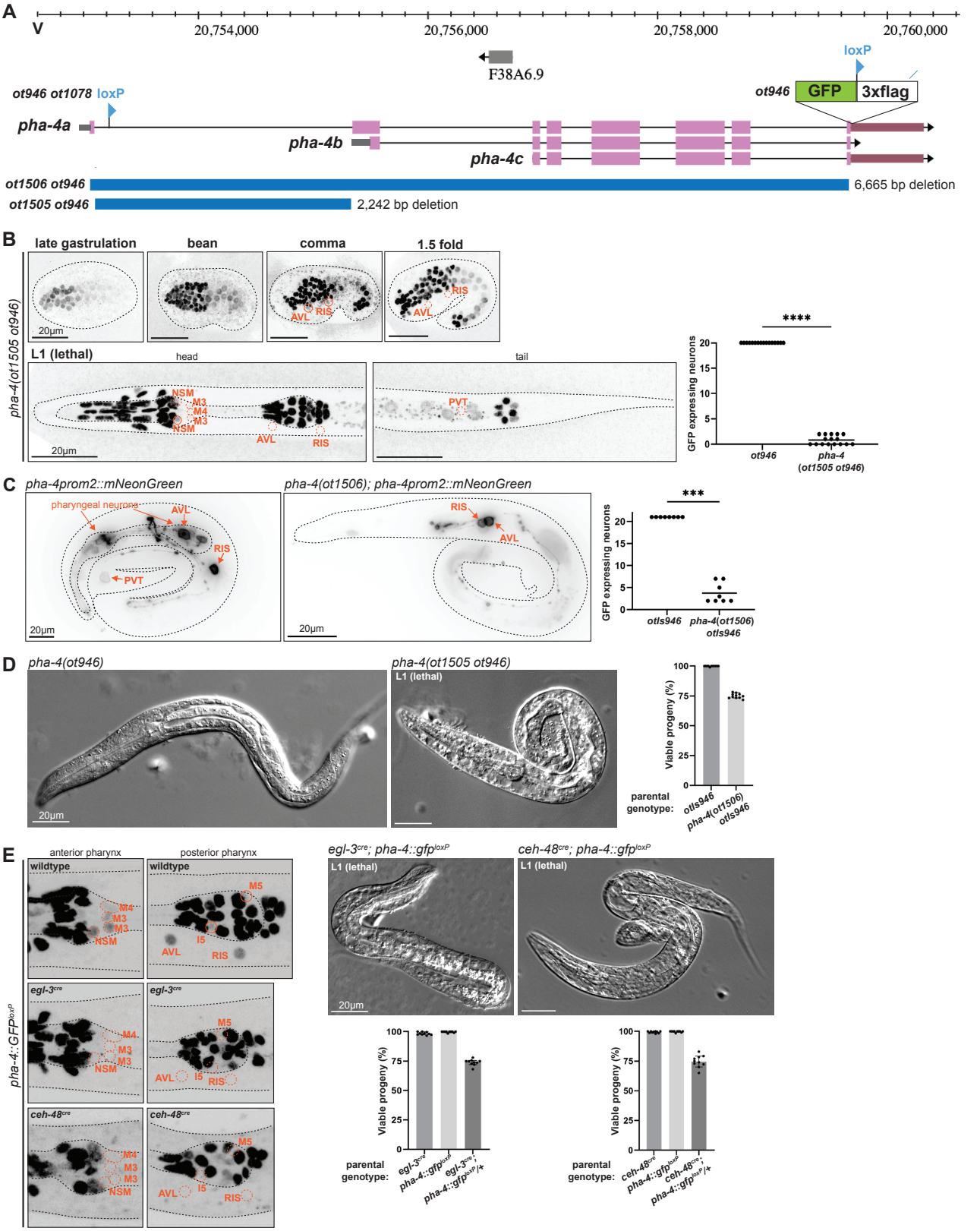

Figure 5: Postmitotic enteric neuron expression of PHA-4 is essential for survival

A: *pha-4* locus schematic on Chromosome V, showing different alleles used in this study.

B: Expression pattern of the *pha-4* cis-regulatory mutant allele (*ot1505 ot946*), showing lack of expression in RIS, AVL, and PVT. All other PHA-4::GFP cells in the head and tail regions of these images are non-neuronal PHA-4(+) cells. The L1 animals are shown from a dorsoventral perspective. Data points representing each individual worm assayed are plotted, and the horizontal line in the middle of the data points represents the median value of biological replicates. **** represents P < 0.0001 in a Mann-Whitney test.

C: Expression pattern of the *pha-4* cis-regulatory allele *pha-4prom2::mNeonGreen::PH::p10 3'UTR* (*otIs946*)*,* in the *pha-4::gfp(ot946)* background with and without full coding region deletion (*ot1506)*. Data points representing each individual worm assayed are plotted, and the horizontal line in the middle of data points represents the median value of biological replicates. *** represents P < 0.001 in a Mann-Whitney test.

D: Bright field image of L1 larva expressing *gfp*-tagged *pha-4* (*ot946* reporter allele)*,* with wildtype morphology (left panel), and of L1 *pha-4(ot1505 ot946)* mutant lethal larva (right. panel). The graph shows the survival rate of the progeny from worms heterozygous for *pha-4(ot1505 ot946)*, in which roughly 25% of worms are homozygous for *pha-4(ot1505 ot946),* 50% are heterozygous for *pha-4(ot1505 ot946),* and 25% are wildtype at the *pha-4* cis-regulatory locus.

E: Left panel**:** neuron-specific depletion of *pha-4::gfp* (*ot946 ot1708*) via *egl-3::Cre* (*syb5804*) and *ceh-48::Cre* (*syb5859*) was confirmed in L1 lethal animals. All remaining PHA-4::GFP cells in the head region are non-neuronal PHA-4(+) cells. Right panel: Bright field images of L1 lethal larva which results upon *pha-4* removal from PENs via the *egl-3::cre*(*syb5804*) or *ceh-48::Cre(syb5859*) drivers. The survival rate of the progeny from worms heterozygous for *pha-4*(*ot946 ot1078*) in the *egl-3::Cre syb5804*) or *ceh-48::Cre*(*syb5859*) driver background, in which roughly 25% of worms are homozygous for *pha-4(ot1946 ot1078),* 50% are heterozygous for *pha-4(ot1946 ot1078),* and 25% are wildtype at the *pha-4* loxP sites.

FIGURE 6

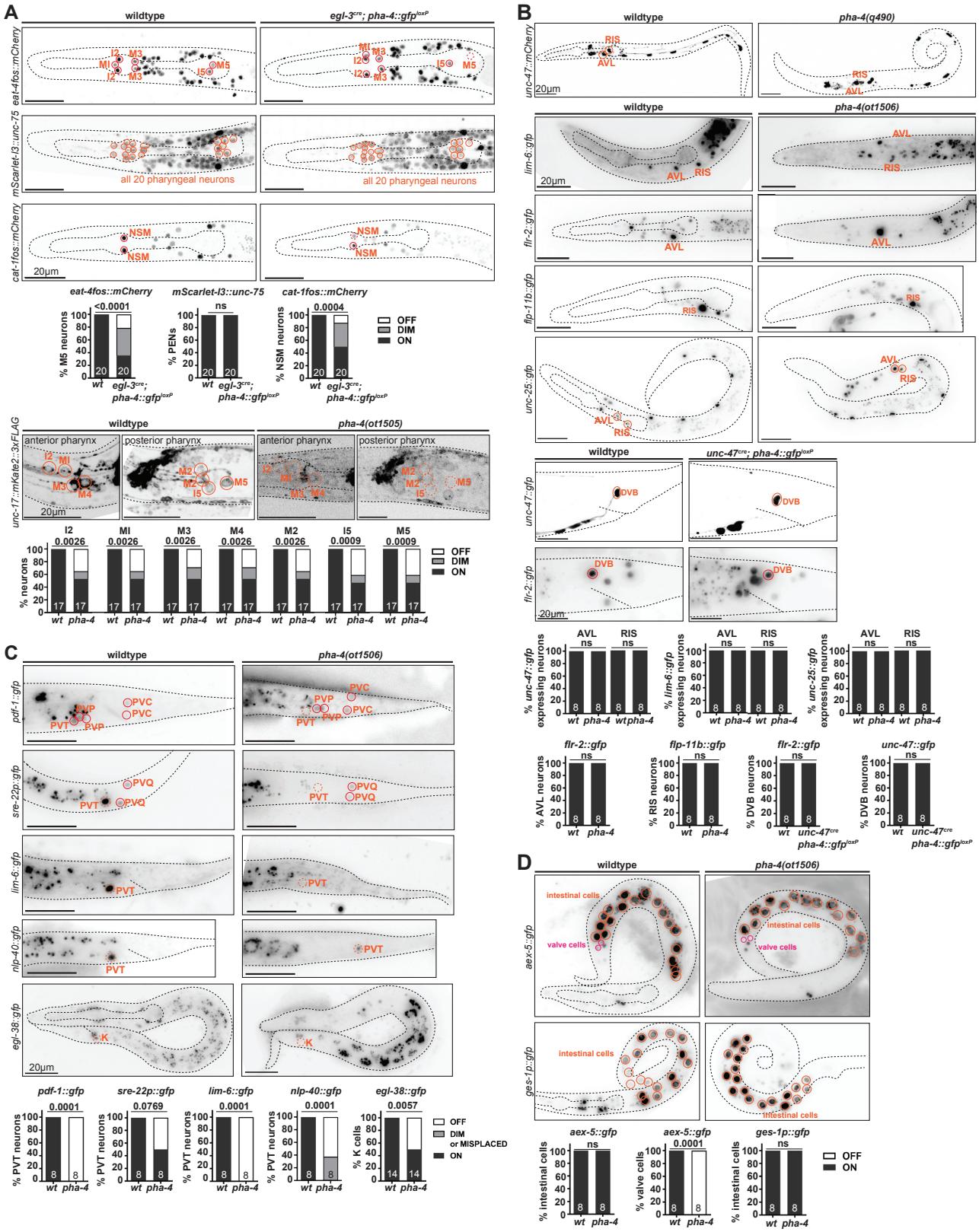
A
wildtype
egl-3cre; pha-4::gfploxP
eat-4fos::mCherry
mScarlet-l3::unc-75
cat-1fos::mCherry
all 20 pharyngeal neurons
NSM
20µm
% M5 neurons
% PENs
% NSM neurons
<0.0001
ns
0.0004
OFF
DIM
ON
wt
egl-3cre; pha-4::gfploxP
unc-17::mKate2::3xFLAG
anterior pharynx
posterior pharynx
pha-4(ot1505)
% neurons
I2 0.0026
MI 0.0026
M3 0.0026
M4 0.0026
M2 0.0026
I5 0.0009
M5 0.0009
pha-4
B
pha-4(q490)
pha-4(ot1506)
unc-47::mCherry
lim-6::gfp
flr-2::gfp
flp-11b::gfp
unc-25::gfp
unc-47::gfp
RIS
AVL
DVB
% unc-47::gfp expressing neurons
% lim-6::gfp expressing neurons
% unc-25::gfp expressing neurons
% AVL neurons
% RIS neurons
% DVB neurons
unc-47cre; pha-4::gfploxP
C
pdf-1::gfp
sre-22p::gfp
nlp-40::gfp
egl-38::gfp
PVC
PVP
PVT
PVQ
K
% PVT neurons
% K cells
pdf-1::gfp 0.0001
sre-22p::gfp 0.0769
lim-6::gfp 0.0001
nlp-40::gfp 0.0001
egl-38::gfp 0.0057
OFF
DIM or MISPLACED
ON
D
aex-5::gfp
ges-1p::gfp
intestinal cells
valve cells
% intestinal cells
% valve cells
aex-5::gfp ns
aex-5::gfp 0.0001
ges-1p::gfp ns

Figure 6: Effect of neuron-specific removal of *pha-4* on PEN & HEN differentiation

A: Loss of *pha-4* affects the expression of neurotransmitter identity genes, but not neuronal identity genes. Images of L1 lethal larva show reporter transgenes *eat-4* (*otIs518*)(Serrano-Saiz et al. 2013), *cat-1 (otIs625*)(Serrano-Saiz et al. 2017), and *unc-75* (*ot1539*)(Cao et al. 2024) in an *egl-3::cre* (*syb5804*) *pha-4::loxP* (*ot946 ot1078*) background. Images of an L1 lethal larva show reporter transgene *unc-17* (*ot907*)(Pereira et al. 2019) in the *pha-4(ot1505)* background. Statistical analysis was performed using Fisher's exact test. N is indicated within each bar and represents the number of neurons scored.

B: Loss of *pha-4* does not affect cell-specific identity genes in AVL, RIS, and DVB. Images of L1 lethal larva show reporter transgene *unc-47* (*otIs348* reporter allele)(Gendrel et al. 2016) in the *pha-4(q490)* background, the *lim-6* (*wgIs387* transgene)(Sarov et al. 2006), *flr-2*(*syb4861* reporter allele)(Vidal et al. 2022), *flp-11*(*ynIs40* transgene)(Kim and Li 2004), and *unc-25*(*ot1372* reporter allele)(Wang et al. 2024) in the *pha-4(ot1506)* background, and *unc-47* (*oxIs12* transgene)(McIntire et al. 1997) and *flr-2*(*syb4861* reporter allele) in the *unc-47::cre*(*arTi479*) *pha-4::loxP* (*ot946 ot1078*) background. Statistical analysis was performed using Fisher's exact test. N is indicated within each bar and represents the number of neurons scored.

C: Loss of *pha-4* affects cell-specific identity genes in PVT and rectal K cells. Images of L1 lethal larva show reporter transgenes *pdf-1*(*syb3330* reporter allele), *sre-22*(*otEx8333* transgene), *lim-6*(*wgIs387* transgene), *nlp-40*(*syb3208* reporter allele), and *egl-38(wgIs171* transgene*)* in the *pha-4(ot1506)* full locus deletion background. Statistical analysis was performed using Fisher's exact test. Sample size is indicated within each bar and represents the number of neurons scored.

D: Loss of *pha-4* does not affect intestine-specific identity genes. Images of L1 lethal larva show reporter transgenes *aex-5*(*ot1532*) and *ges-1*(*otIs904*)(Sural et al. 2025) in the *pha-4(ot1506)* background. Statistical analysis was performed using Fisher's exact test. N is indicated within each bar and represents the number of animals scored.

FIGURE 7

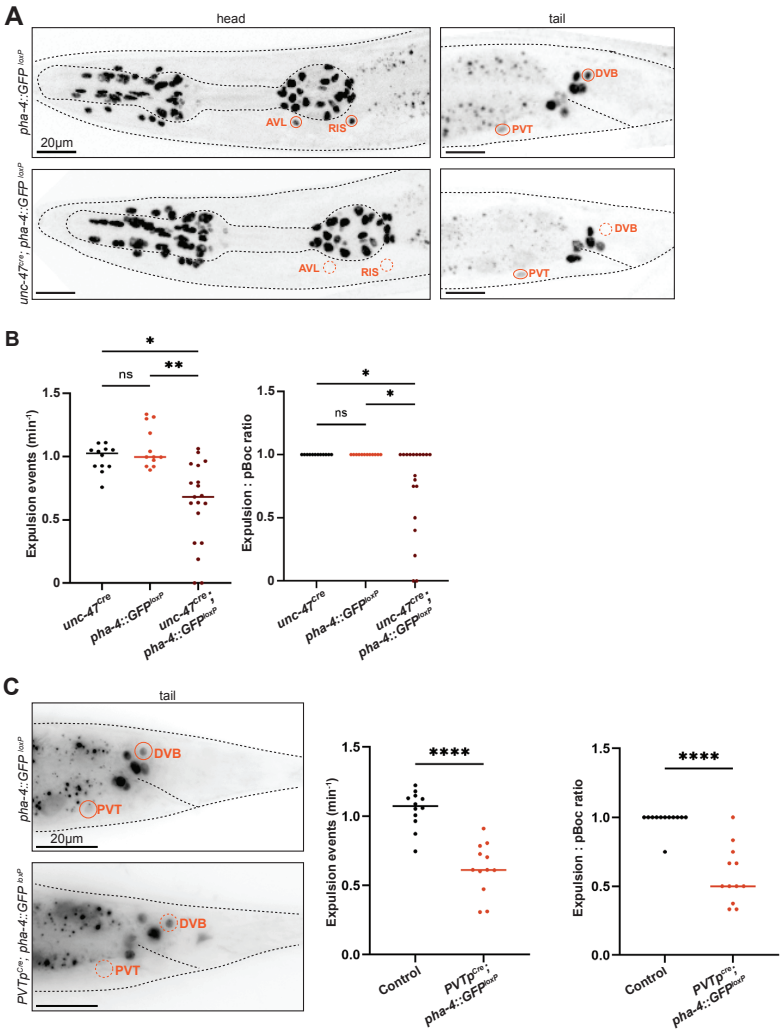

Figure 7: *pha-4* acts in HENs to control defecation behavior.

A: Cell-specific removal of *pha-4* expression (*ot946 ot1078*) via *unc-47::cre*(*arTi479*). Animals were scored at the day 1 adult stage.

B: *pha-4* removal from AVL, RIS, and DVB affects defecation behaviour. Frequency of expulsion and expulsion : pBoc ratio in adult worms with cell-specific removal of pha-4 expression (*ot946 ot1078*) via *unc-47::cre*(*arTi479*).

C: Left panel: neuron-specific depletion of *pha-4::gfp* (*ot946 ot1708*) via *sre-22::Cre* (*otEx343*) was confirmed in adult animals. All remaining PHA-4::GFP cells in the tail region are non-neuronal PHA-4(+) cells. Right panel: *pha-4* removal from PVT affects defecation behavior. Frequency of expulsion in adult worms with PVT-specific removal of *pha-4* expression (*ot946 ot1078*) via PVT::cre (*otEx343*). Expulsion : pBoc ratio in adult worms with PVT-specific removal of pha-4 expression (*ot946 ot1078*) via PVT::Cre (*otEx343*).

Data points representing each individual worm assayed are plotted, and horizontal line represents median value of biological replicates in (B-C). *, **, **** and ns represent $P < 0.05$, $P < 0.01$, $P < 0.0001$ and not significant, respectively, in Dunn's multiple comparison test after Kruskal-Wallis test (B), and Mann-Whitney test (C).

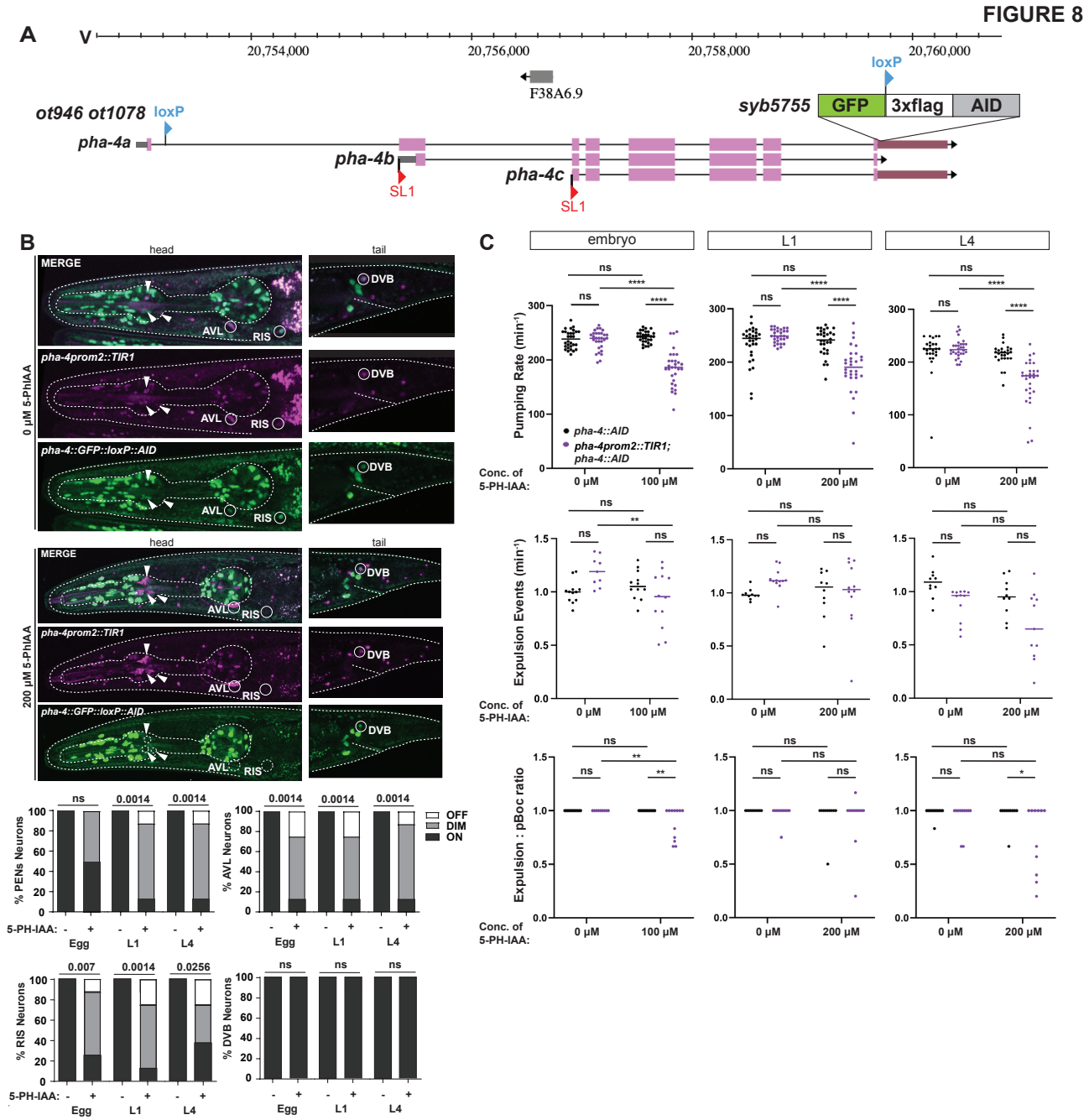

Figure 8: *pha-4* is continuously required in enteric neurons to maintain function.

A: *pha-4* locus schematic showing the *pha-4* CRISPR/Cas9 engineered AID tag (*ot946 ot1078 syb5755*).

B: Temporally controlled removal of *pha-4*(*ot946 ot1078 syb5755)* from enteric neurons via *TIR1(F79G)*(*otIs908*) in the presence of 5-Ph-IAA. Animals were treated with either ethanol only (0 µM 5-Ph-IAA) or 200 µM 5-Ph-IAA, starting at various stages, and GFP expression in *pha-4(+)* neurons were characterized. White arrows point to *TIR1(F79G)* and *pha-4*(*ot946 ot1078 syb5755)* expression in pharyngeal neurons. Statistical analysis was performed using

Fisher's exact test. N is indicated within each bar and represents the number of neurons scored.

C: Temporally controlled removal of *pha-4* from enteric neurons results in defects in enteric behaviors. Pharyngeal pumping, frequency of expulsion, and expulsion:pboc ratio in adult worms treated with auxin starting at different developmental stages. Animals were treated with either ethanol only (0 μM 5-Ph-IAA) or indicated concentrations of 5-Ph-IAA. Data points representing each individual worm assayed are plotted, and the horizontal line represents the median value of the biological replicates in (C-D). *, **, **** and ns represent $P < 0.05$, $P < 0.01$, $P < 0.0001$ and not significant, respectively, in Sidak's multiple comparisons test after two-way ANOVA (C), and a Mann-Whitney test (D).